AN ABSTRACT OF THE THESIS OF

Suzanne Mirashrafi for the degree of Master of Science in Materials Science presented on November 29th, 2016.

Title: Photoinitiated Grafting of PMMA onto Cellulose Nanocrystals to Improve Nanocomposite Reinforcement-matrix Interface

Abstract approved:

_____

John Simonsen

Cellulose nanocrystals (CNCs) are extremely abundant, biodegradable and light weight nanoparticles that have the potential to contribute in many fields including packaging, construction, solar cells and automotive. With the increasing interest in nanotechnology and nanocomposites, CNCs could provide a renewable, optically transparent and strong alternative to other nano-scale reinforcement phases. One challenge that limits the applications of CNCs in polymer composites is that the hydrophilic nanocrystals have poor dispersion and interfaces with hydrophobic polymer matrices. This project worked to improve the compatibility of CNCs with polymer matrices, specifically poly(methyl methacrylate) (PMMA). This was done by first immobilizing a UV-photoinitiator to the surface of the nanocrystals and then grafting PMMA from the CNCs surface using radical photopolymerization.

It was found that the concentration of the immobilized initiator could be controlled using the length of the reaction. The photopolymerization with initiator modified CNCs successfully resulted in PMMA-grafted CNCs (CNC-g-PMMA), with up to 66% w/w PMMA covalently bonded to the cellulose surface. FTIR, DSC, TGA and elemental analysis all showed that CNC-g-PMMA had properties that were in between those of PMMA and ungrafted sulfonated CNCs

(s.CNCs). When PMMA composites were made with ungrafted s.CNCs and CNC-g-PMMA, their properties were compared to each other and to those of neat PMMA. Optically, composites with both forms of CNCs were comparable to PMMA at around 1% w/w, however became cloudy at higher concentrations. The Young's moduli of CNC-g-PMMA composites of 4% w/w CNCs or less were higher than those of s.CNC composites. These CNC-g-PMMA composites also had higher interface values when fit with the Shear-Lag Capped (SLC) model than the s.CNC composites. At higher concentrations of CNCs both types of composites showed reduced mechanical properties, most likely due to nanoparticle agglomeration and poor dispersion.

Photoinitiated Grafting of PMMA onto Cellulose Nanocrystals to Improve Nanocomposite Reinforcement-matrix Interface

by

Suzanne Mirashrafi

A THESIS

submitted to

Oregon State University

in partial fulfillment of
the requirements for the
degree of

Master of Science

Presented November 29, 2016
Commencement June 2017

Master of Science thesis of Suzanne Mirashrafi presented on November 29, 2016.

APPROVED:

_____

Major Professor, representing Materials Science

_____

Head of the School of Mechanical, Industrial and Manufacturing Engineering

_____

Dean of the Graduate School

I understand that my thesis will become part of the permanent collection of Oregon State University libraries. My signature below authorizes release of my thesis to any reader upon request.

_____

Suzanne Mirashrafi, Author

ACKNOWLEDGEMENTS

I would like to thank my parents, Mojy and Jacqui, for being so incredibly supportive and encouraging. They taught me to have confidence and resilience through good days and bad days. Thank you to my best friend, my sister Sophia, for her wit and distracting book recommendations.

I would also like to express my gratitude to my mentor, Dr. Simonsen, for giving me the opportunity to learn such an expansive breadth of skills and knowledge. It has been an education that will serve me for the rest of my career and life.

I would also like to thank my Graduate Committee: Dr. David Cann, Dr. Skip Rochefort and Dr. Laurence Schimleck for their time.

Thank you to the countless teachers and coaches at Oregon State University who shared their expertise with me, including Dr. Bill Warnes, Teresa Sawyer, Dr. Pete Eschbach, Dr. Meisam Mohammadi, Steve Huhn, Dr. Jessica Vellucci, Dr. Miguel Goñi, Dr. Christopher Beaudry, Dr. Skip Rochefort, Brit Swann, Steph Walker and Dr. Joan Hudson.

To Paige, Jessica and Jenna, it was a pleasure experiencing graduate school with you.

TABLE OF CONTENTS

LIST OF FIGURES

LIST OF FIGURES (CONTINUED)

LIST OF TABLES

Photoinitiated Grafting of PMMA onto Cellulose Nanocrystals to Improve Nanocomposite Reinforcement-matrix Interface

CHAPTER 1: INTRODUCTION

1.1 Motivation

Polymers and polymer composites have become integral in most aspects of our daily lives. They make up a significant portion of the materials in our vehicles, technological devices, food packaging and furniture. The recent movement towards greater environmental responsibility has increased the demand for more sustainable materials and less toxic production processes. Cellulose nanocrystals (CNCs) have gained a great deal of attention for their potential as a renewable, lightweight, strong and transparent material that could fulfil this demand in forms such as nanofillers in polymer nanocomposites [1]. However, there remain some challenges when using nanocellulose in polymer composites such as poor nanoparticle dispersion within the matrix and imperfect compatibility between the phases of the composite.

The purpose of this research was to develop a method of modifying the surface of CNCs to enhance the interface between the matrix and reinforcement phases of CNC/polymer composites and, as a result, improve the strength and clarity of the materials. This was accomplished by grafting hydrophobic poly(methyl methacrylate) (PMMA) chains from the surface of the CNCs using UV light activated radical polymerization. Photoinitiation was selected as the method of polymerization because it requires less initiation energy and affords greater spatial and temporal control over the reaction than traditional heat activated radical polymerization reactions [2].

PMMA was chosen as the grafting and matrix polymer because of its excellent optical clarity and diverse range of potential applications. Finally, in order to ensure that this process could be applicable to an industrial scale, a small-scale spinning disk reactor was investigated as a potential process intensification tool.

1.2 Cellulose nanocrystals

1.2.1 General introduction to cellulose

As the most abundant biopolymer on earth, cellulose has great potential for meeting the rising demands from consumers, governmental agencies and businesses for more sustainable alternatives to materials derived from non-renewable resources like petroleum. Cellulose is found in a wide range of sources including wood, plants (cotton, hemp, flax, grasses, etc.), marine animals (tunicates), algae and bacteria [3]. For centuries cellulose has been utilized by humans in numerous practical applications including construction, textiles and writing material [4].

Cellulose is a linear polysaccharide chain of anhydroglucose rings connected by β-(1,4)-glucosidic bonds. The repeat unit of cellulose is defined as two glucose sugars with each anhydroglucose ring oriented 180^{o} from its neighboring monomer [Figure 1].

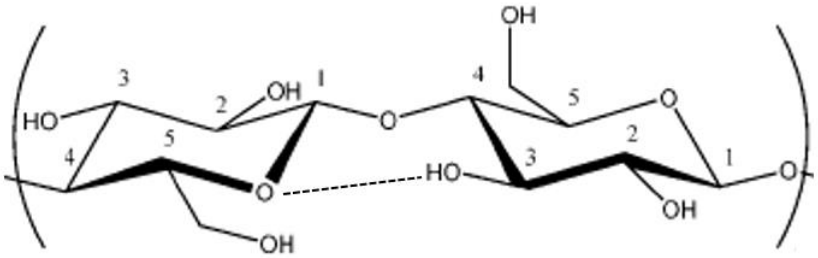

Figure 1. Repeating unit of cellulose polymer, showing two anhydroglucose rings connected by β-(1,4)-glucosidic bonds and intra-chain hydrogen bonding (dashed line). Image modified from [5]

The corkscrewed orientation of the monomers allows for stabilizing intra-chain hydrogen bonding between the O5 within one ring and the hydrogen on the C3 hydroxide of the next ring, giving the cellulose its ribbon-like form and stiff mechanical properties [3]. These biopolymers are organized into small bundles of parallel chains called elementary fibrils, which further combine to form microfibrils. Within the fibrils are crystalline regions of highly aligned, closely packed cellulose chains. These crystalline regions are connected by amorphous areas that contain kinks and bends that prevent close packing [3]. The composition and structure of cellulose allows it to participate extensively in hydrogen bonding, not just within and between chains, but also with surrounding solvents, giving cellulose its highly hydrophilic nature.

1.2.2 Cellulose nanocrystals

Nanoscience and nanotechnology are the study and application of materials with at least one dimension that is 100nm or smaller [6]. In 1959, Richard Feynman expressed his belief that progress lies in making things smaller and smaller. He marveled at the efficiency of biological systems despite how “exceedingly small” they are and urged his audience to “[c]onsider the

possibility that we too can make a thing very small which does what we want – that we can manufacture an object that maneuvers at that level" [7]. Feynman also observed that materials do not act in nanoscale as they do in macroscale or even microscale. For example, gold nanoparticles appear red when they interact with visible light, as opposed to the characteristic yellow the metal is known for. Commonly researched nanoparticles include gold, silver, carbon nanotubes and semiconducting materials. A great deal of interest and progress has grown from this concept that smaller particles of material will exhibit new and exciting properties that can be exploited in fields such as material science, computer science, molecular chemistry, quantum physics and medicine [8].

While the majority of materials considered for nanotechnological applications are either synthesized or manufactured to create nanoparticles, the native structure of cellulose gives it the unique potential to be a sustainable and biodegradable nanomaterial that can be isolated from its natural form. In 1947, R.F. Nickerson and J.A Habrle observed that treating cellulose fibers with boiling acid resulted in the degradation of the material [9]. CNCs were first reported in the 1950s by the Swedish polymer chemist, Bengt Ranby, who observed a colloidal suspension of cellulose after degrading cellulose fibers in sulfuric acid [5].

CNCs have gained an increasing degree of attention in research and industry in the last few decades, which is reflected in the increasing number of patents and articles submitted each year [1]. CNCs are made by isolating the nano-sized crystalline regions of cellulose through the erosion of the connecting amorphous regions. First, cellulose is usually purified of any other compounds found in the fibers from the source, such as lignin and hemicellulose in wood. The crystalline regions are then isolated either through mechanical processing or, more commonly, through acid

hydrolysis. These treatments degrade the weaker amorphous regions, leaving the more durable crystalline areas intact [3]. In acid hydrolysis, the acid has greater access to destroy the loosely-packed amorphous chains but will not easily penetrate the closely-packed crystals [10]. The resulting crystals are needle-like and have been described with names such as cellulose nanocrystals, cellulose nanofibers and cellulose whiskers. Transmission electron microscopy (TEM) is often used to characterize the dimensions and shape of CNCs [Figure 2].

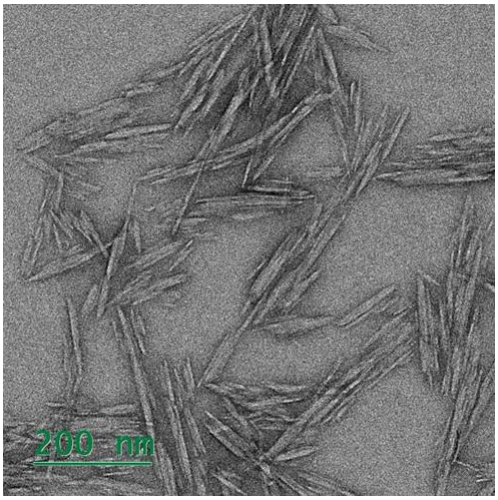

Figure 2. TEM image of cellulose nanocrystals from wood source

The dimensions of the CNCs that remain after the acid hydrolysis can depend on the original source of the cellulose [Table 1].

Table 1. Dimensions of CNCs from different cellulose sources [10]

Source of Cellulose	Length (nm)	Cross Section (nm)
Tunicate	100-several 1000	10-20
Bacterial	100-several 1000	5-10 by 30-50
Algal	>1000	10-20
Cotton	200-350	5
Wood	100-350	3-5

Cellulose nanocrystals are light, strong, nontoxic and biodegradable. The nanocrystals are stronger than bulk cellulose because the weak amorphous regions have been removed to leave only stiff crystals with very high aspect ratios [11]. The physical properties of CNC are very impressive when compared to other frequently used engineering material [Table 2].

Table 2. Properties of composite reinforcement materials compared to CNCs [3]

Material	Density (g/cm^3)	Strength (GPa)	Modulus (longitudinal) (GPa)	Modulus (Transverse) (GPa)
CNC	1.6	7.5-7.7	110-220	10-50
Kevlar-49 fiber	1.4	3.5	124-130	2.5
Carbon fiber	1.8	1.5-5.5	150-500	-
Steel wire	7.8	4.1	210	-
Carbon nanotubes	-	11-63	270-951	0.8-30

The nanoscale size of the crystals results in a unique transparent property because the dimensions of the crystals are small enough to minimize the scattering of light as it passes through the particles [12]. There are many applications in packaging and reinforced composites that could exploit the strength, stiffness and transparency of CNCs. The exceptional properties of CNCs have captured the interests of fields such as nanocomposites, optical applications, barrier films, drug delivery and many other areas of nanotechnology [11].

1.3 Poly(methyl methacrylate)

PMMA, a synthetic thermoplastic, was first discovered by British chemists Rowland Hill and John Crawford in the early 1930s [13]. In 1934, Otto Rohm, a German pharmacist and chemist, patented a polymerization process of PMMA and created the brand Plexiglas [14]. In addition to Plexiglas, PMMA has also been known as Acrylite and Lucite. PMMA is lightweight, optically clear and resistant to shattering, weathering and scratching [13]. These properties have made PMMA very useful as an alternative to inorganic glasses in applications such as cars, airplanes, packaging and displays. One of the first major uses of PMMA was for airplane windows during World War II. PMMA has also been found to be biocompatible with human tissues, further opening the range of potential uses in medicine. Modern applications of PMMA are in areas such as biomedical, drug delivery, automotive, solar, sensor and nanotechnological fields [13], [15].

PMMA is synthesized from its monomer, methyl methacrylate (MA) [Figure 3].

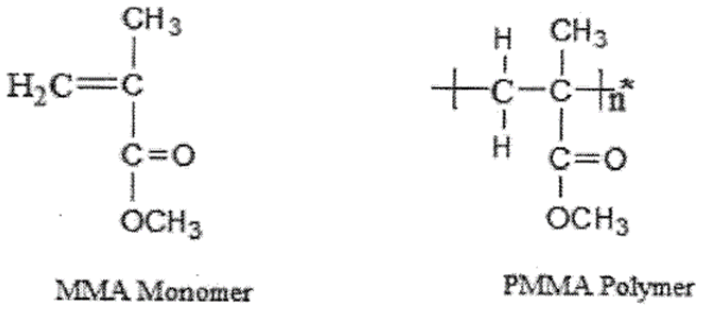

Figure 3. Methyl methacrylate monomer and poly(methyl methacrylate) polymer repeat unit [13]

PMMA is made with a variety of techniques, including free radical and anionic-initiated polymerization in bulk, solution, suspension and emulsion methods [13]. PMMA is an amorphous polymer because the bulky methyl group prevents the chains from packing closely. The physical and mechanical properties of PMMA are summarized in Table 3.

Table 3. Properties of PMMA [13]

Property	PMMA
Color	Colorless
Density	1.18 g/cm^3
Melting point	220-240℃
Glass Transition Temperature (T_g)	110-120℃
Water Absorption	0.3%
Surface Hardness (Rockwell)	M90-M100

1.4 Photopolymerization

Polymerization is the reaction that links individual monomers to form long polymer chains and it can be performed with a variety methods. Frequently used techniques include ionic, coordinated-complex catalyzed, ring-opening and free radical polymerizations [16]. Free radical polymerization is a reaction initiated with the formation of extremely reactive free-radical species. The three steps of a free radical reaction are (1) the initiation of the radical species, (2) the propagation of the radical species, which is responsible for the addition of monomers to the polymer chain and (3) the termination of the radical species [Figure 4]. Radical reactions can also be used for crosslinking low-molecular weight oligomers into high-molecular weight polymer networks in a process called curing [17].

Step 1: *Initiation*

$\text{Initiator} \rightarrow R^{\bullet}$

$R^{\bullet} + M \rightarrow M_1^{\bullet}$

Step 2: *Propagation*

$M_1^{\bullet} + M \rightarrow M_2^{\bullet}$

$M_2^{\bullet} + M \rightarrow M_3^{\bullet}$

$M_x^{\bullet} + M \rightarrow M_{(x+1)}^{\bullet}$

Step 3: Termination

$M_x^{\bullet} + M_y^{\bullet} \rightarrow M_{(x+y)}$ *Coupling*

$M_x^{\bullet} + M_y^{\bullet} \rightarrow M_x + M_y$ *Disproportionation*

Figure 4. Radical polymerization schematic [16]

The radical species can be initiated with a range of compounds and techniques. Peroxides and hydrogen peroxides are commonly used initiators that will decompose into radical molecules when exposed to heat. Vinyl monomers, such as styrenes, can form radicals under elevated thermal conditions without additional initiators. While thermally-initiated polymerizations are very popular and useful, light-initiated free radical compounds, also called photoinitiators, have many benefits over conventional methods. It is easier to regulate the exposure area and time with light in a reaction than it is with heat in order to control the duration of the reaction and the properties of the product [2].

Type I photoinitiators, including many peroxide, disulfide, benzoin and benzyl compounds, are a category of initiator that only require a single compound that is activated by light energy [16]. Type II photoinitiated systems involve one compound that is excited into a higher state by light that then activates a second co-initiator to form a radical, which then propagates the growth of the polymer chain [2], [18].

1.5 Nanocomposites

1.5.1 General background of composites

Engineered composites are a class of man-made materials that consist of at least two dissimilar phases. The phases usually fall into two general categories: matrix and reinforcement. The matrix is a softer, continuous phase that serves to protect and transfer the load to the reinforcement phase. Matrices include diverse materials such as thermoplastic polymers, cross-linked thermoset polymers, metals and ceramics. The reinforcement phase is a much stronger, stiffer material that can come in the form of long fibers, chopped/short strands or nanoscale particles. Reinforcement materials include fiber glass, carbon fibers, wood, aramid polymers and inorganic oxides [19].

Some of the most intricate examples of composite-like materials can be found in nature. Wood, for instance, can be considered a composite with the lignin matrix encasing the stiff fibrils of cellulose. Man-made composites have been utilized by humans in structures for centuries, for example using straw reinforcements in clay or mud matrices to construct dwellings. Plywood, wood reinforcement in an adhesive matrix, is another popular composite used in construction. Composites are attractive materials because they allow for a great deal of control in the design of mechanical properties and the incorporation of raw materials that might not be useable in other forms, for example nano-sized filler materials. The selection of matrix and reinforcement materials and the concentration, orientation and form of the reinforcement phase all make it possible to tailor the overall properties. Anisotropic strength, stiffness, density and thermal stability can all be adapted to fit the final use of the product [19]. Within the last few decades, the use of polymers,

carbon fibers and glass fibers have become popular in aerospace and automotive industries to meet the demand for lighter and stronger products.

In order for composites to be useful materials, they must act as closely to a coherent material as possible when applied with a load, rather than two mixed-yet-separate materials. The composite is able to act as a coherent material when the reinforcement phase and matrix interact strongly at the interface. Poor interface between the phases can result in slipping, debonding or cracking, which can diminish the composite's properties because the load cannot be properly transferred from the matrix to the stronger reinforcing fibers. This is a problem that frequently plagues composites that have incompatible phases, such as hydrophilic cellulose in a hydrophobic polymer matrix. Methods of improving interphase interactions include electrostatic attraction, covalent bonding, mechanical keying and surface modifications [20]. The preferable method of improving interphase interactions is highly dependent on the form and types of materials in the composites.

1.5.2 Nanocomposites

With the recent increased understanding and interest in the unique properties of nanoscale materials, scientists and researchers have begun to investigate the potential of nano-sized reinforcement phases in composites. However, while the field of research in nanotechnology is relatively new, nanocomposites themselves are not. The vibrant red color of stained glass windows dating back as early as the 4th century come from colloids of copper and gold nanoparticles [21]. Carbon black, amorphous silica and exfoliated clays are all nano-sized fillers that had been used

decades before nanocomposites and nanotechnology developed as a formal field of study. Modern nanocomposites include nanoclay in nylon matrices, carbon nanotubes in polymer composites and graphite in silicone/epoxy matrices [21].

Nanocomposites are on the verge of becoming an incredibly important part of industries such as automotive, aerospace, electronics, energy and construction. The polymer nanocomposite market is expected to reach $5100 million globally by 2020 [21]. Nanocomposites have the potential of improved tensile strength, higher heat distortion temperatures, better optical clarity, increased melt viscosities and greater toughness compared to conventional composites [21]. They can also be made with many manufacturing processes frequently used for unfilled polymers such as injection molding, thermoforming, extrusion and compression molding, which can be difficult with conventional composites.

While there are many advantages for polymer nanocomposites, there remain a few prominent challenges. First, as with conventional composites, the nanoparticle reinforcement phase can have poor compatibility and interface with the continuous matrix. This can lead to agglomeration and insufficient dispersion of the reinforcement within the matrix. Agglomeration of nanoparticles increases the size of the reinforcement material, reducing the nanoscale characteristics of the particles. Second, nanocomposites remain relatively expensive to produce because few processes have been developed to make nanoparticles of many materials affordable on an industrial scale [21].

1.6 Spinning disk reactor

The success of a material in industry is dependent on how reliably it can be scaled-up in production while maintaining the cost-effectiveness and the quality of the product. Historically, scaling-up production has been achieved with larger batches [22]. There are many limitations to this method of increased production including difficulty mixing, poor heat transfer, limited control over reaction conditions and high-risk of invested cost and materials should a large batch fail. This form of scaling-up limits the types of reactions that can be used, for example eliminating highly exothermic reactions or light-initiated polymerizations. Process intensification is a means of scaling-up a reaction without the need to increase the volume the batch itself. It can minimize the size and complexity of the system, improve the yield of a reaction, reduce energy cost, decrease reaction time and be carried out in smaller, safer volumes at a given time. Process intensification can be achieved by modifying a variety of aspects of the reaction itself, including using alternative energies, novel methods of reaction or different types of reactors [22].

An example of an alternative form of reactor that has grown in acceptance in both industry and academia is the spinning disk reactor [Figure 5]. As shown in Figure 5, a spinning disk reactor is composed of an enclosed rotating disk in which the atmosphere, reaction temperature, light exposure and flow-rate of the solution can be tightly controlled. The solution is deposited close to the center of the disk and flows across the surface in a highly-sheared thin film. The shear is caused by the tangential stress between the disk and the liquid as the film is spun off of the disk through centrifugal acceleration [22]. The thin dimension of the film and the excellent thermal conductivity of the disk make it possible for efficient heat transfer.

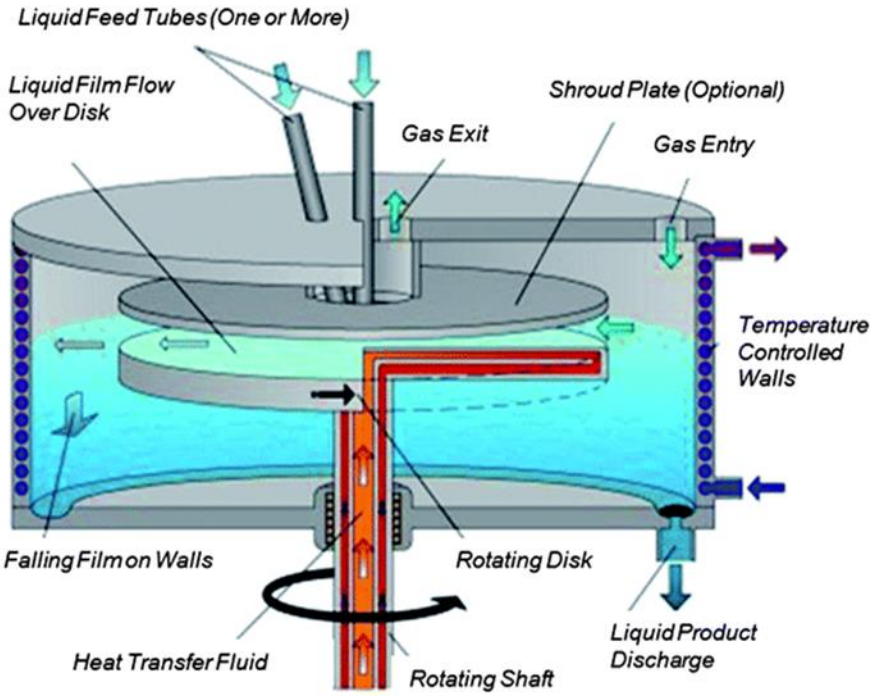

Figure 5. Schematic of spinning disk reactor. Image from [22]

The thickness of the film and the residence time of the reaction on the disk can be controlled with variables like the rotational speed of the disk and flow rate of the solution [22] [Eq. 1 and 2].

$$\text{Film thickness (m): } f = \left(\frac{3\nu Q}{2\pi\rho r^2\omega^2}\right)^{1/3} \quad \text{[Eq.1]}$$

$$\text{Mean residence time(s): } t = \left(\frac{81\pi^2\nu}{16\rho Q^2\omega^2}\right)^{1/3} r^{4/3} \quad \text{[Eq. 2]}$$

where ν, Q, ρ, r, ω and f are liquid viscosity (Pa s), liquid flow rate (m^3/s), liquid density (kg/m^3), disk radius (m), rotational speed of the disk (radian/s) and film thickness (m), respectively. By controlling the residence time, many reaction variables can be manipulated, such as the exposure to light for light-initiated reactions. Reactions performed on the spinning disk reactor have had products that are comparable or better than traditional bulk methods [23]. The spinning disk reactor has been used for the syntheses of small inorganic particles like barium sulfate and calcium

carbonate, the polymerizations of polyurethane and polystyrene and the production of metal nanoparticles. The spinning disk reactor has proven to be especially well suited for polymerizations [24].

CHAPTER 2: LITERATURE REVIEW

2.1 Cellulose

2.1.1 Nanocellulose composites

CNCs are quickly becoming recognized as a renewable and versatile option for reinforcements phases in nanocomposites [11], [25]. Cellulose nanofibers (CNFs) and CNCs have high aspect ratios and are extremely light and strong, which is ideal for composite reinforcement phases. Also, while many commonly used nanoparticles have raised concerns of toxicity, CNCs have been shown to be nontoxic and are even used in food packaging [26] and biomedical applications [27]. The first reported CNC composite was by Favie et al., in a latex matrix in 1995 [28]. Composites utilizing CNCs have been made with a range of polymers, such as PMMA, polysulfonates, polysiloxanes, poly(caprolactones), cellulose acetate butyrate, epoxides, polyethylene, polypropylene and polyurethane, among many others [5]. CNC nanocomposites have the potential of remaining optically clear while being stronger and stiffer than unfilled materials, even at low filling percentages [5], [11].

CNC/PMMA composites have recently gained attention as an interesting nanocomposite because both components of the composite have excellent optical clarity, which could have many exciting applications in solar cells, windows, alternative building materials and automobiles [29]. Li et al. developed a CNC/PMMA nanocomposite by removing the lignin from wood while maintaining the nanoporous structure of the wood cell walls to create "optically transparent wood" [29]. The delignified wood was then impregnated with MMA and heated until the matrix polymerized. The delignified wood only became transparent after the addition of the PMMA matrix because PMMA reduced the light scattering and regulated the optical interface. Mechanically, the 5% v/v cellulose composite had a higher elastic modulus (2.05 GPa) than both PMMA alone (1.8 GPa) and delignified wood alone (0.22 GPa). When compressed to give 19% v/v cellulose volume, the composite was twice as strong as neat PMMA.

Dong et al. applied the fabrication technique of electrospinning to CNC/PMMA nanocomposites to create sub-micron fibers ranging from 0% to 41% w/w CNC [30]. The authors acknowledged the difficulty of achieving good dispersion of CNC in nonpolar solvents. They found that N,N-dimethylformamide (DMF) allowed for both the good dispersion of CNCs and the dissolution of PMMA, however this could limit the other material systems this method could be applied to. The resulting composite fibers had highly aligned nanocrystals within the PMMA matrix. The glass transition temperature (T_g) of the composites were slightly higher than that of neat PMMA, however did not vary much as the amount of CNCs in the composite increased. Threads of at least 17% w/w CNC showed an average increase of 0.9 GPa, or 17% increase, in storage modulus (E') compared to neat PMMA when tested in the transverse direction with nano-dynamic mechanical analysis (nano-DMA). Since the crystals were aligned in the axial direction,

it is possible there could be greater improvement in mechanical properties in that direction; however the authors were not able to test this. Electrospinning of CNC/PMMA composites appears to be a promising means of incorporating CNC into thread nanocomposites, however more mechanical testing should be done on a useable form of the composite, such as in a spun mat. Also, while the dispersion and alignment of the CNCs were measured, there was no characterization of the interface between the phases.

Transparent CNC/PMMA films, as well has bacterial nanocellulose/PMMA and nanofibrillated cellulose/PMMA films, have been made using acetone solvent casting methods with cellulose loads of only 0.25% to 0.5 % w/w [31]. These films exhibited slight increases in flexural strength and improved storage modulus compared to neat polymer. Transparency was only maintained at lower concentrations of cellulose before the films became visibly cloudy and decreased in percent transmittance in the UV and visible light ranges. The reduced clarity could have been caused by agglomeration due to poor dispersion of the hydrophilic nanoparticles in the hydrophobic matrix.

The literature of cellulose composites show that CNC/polymer composites are growing in popularity and interest because of their transparency and improved mechanical properties. The majority of the research done has been with CNCs in PMMA matrices. One of the greatest limitations of CNC/polymer composites is the hydrophilicity of the crystals compared to the hydrophobic nature of polymer matrices. This causes poor dispersion of the nanocrystals in the matrix, which could lead to cloudiness due to agglomeration and limit the amount of CNCs that can be constructively loaded into the composite. It could also be challenging to find a solvent that both matrix and cellulose can be well dispersed in due to differences in polarity and solubility.

This challenge to produce successful composites can be addressed by modifying the surface chemistry of the cellulose to become more hydrophobic [32].

2.1.2 Modification of cellulose nanocrystals

While CNCs possess great potential in a variety of applications, the use of the nanocrystals are often limited by the hydrophilic nature of their surfaces, causing incompatibility with other materials or solvents. The abundant hydrogen bonding on the nanocrystals' surfaces is responsible for their hydrophilicity and high surface energy, leading to the agglomeration of the crystals. Agglomeration causes poor dispersion and can reduce the benefits of the nanoscale dimensions. These limitations can be remedied with the modification of the surface of CNCs by covalently bonding or adsorbing different compounds to the crystals. Cellulose has three hydroxyl groups: two secondary groups on the C2 and C3 of the glucose ring and a third primary group on the C6. The secondary hydroxyls groups are much slower to react than the C6 hydroxyl group, resulting in the majority of the reactions occurring at the primary hydroxyl. Research with esterification reactions indicate that the primary hydroxyl can react as high as ten times faster than the other two hydroxyls [33].

Research has been focused on a variety of modifications of cellulose in the forms of filter paper [34]–[37], cotton fabrics [36], [38], cellulose powder [39]–[41] and microcrystalline cellulose [42]. Less research has been done on the modification of CNCs [43]–[45]. A wide range of chemical alterations have been performed with the primary hydroxyl groups on the cellulose surface, including sulfonation, oxidation, cationization and silylation [43]. Carboxyl groups are

often attached to the surface of CNCs in order to increase the surface charge and discourage agglomeration in aqueous solutions [11]. Cellulose fibers have been modified in order to develop antimicrobial and fire retardant properties [46]. Metal nanoparticles have been bonded onto CNC surfaces to act as a supports for enzymes in biochemical applications [43]. CNCs also have been modified with unsaturated compounds, such as maleic anhydride, so that they can participate in cross-linking in CNC/polymer composites [11].

Another useful modification of cellulose is the grafting of polymer chains onto the surface of the cellulose fiber or crystal. By covalently bonding long, nonpolar molecules to the normally hydrophilic surface, the cellulose itself becomes much more hydrophobic [44]. This change in surface chemistry can improve the dispersion of the material in nonpolar solvents and strengthen the matrix-reinforcement interface in cellulose/polymer composites. The interface is improved because the polymer chains covalently bonded to the cellulose surfaces will interact and entangle with the other hydrophobic chains of the matrix. A polymer can be attached to the surface of another polymer either by "grafting onto" or "grafting from" the surface [47]. "Grafting onto" refers to the process of connecting two fully polymerized chains with reactive end groups. "Grafting from" occurs when the monomer of the grafting co-polymer grows from an active site on an existing polymer backbone. "Grafting from" is the most commonly used technique in cellulose modification because it provides the highest efficiency of grafting [48].

Some researchers have attempted to graft polymers to cellulose by simply having the cellulose material present in solution with the monomer and radical initiators during the polymerization. However, this gives very little control over the molecular weight or amount of grafted polymer chains on the nanocrystals [39], [40], [42]. Since there are no sites on the cellulose

that have been activated to increase the participation of the nanocrystals in the radical polymerization, it is possible that the reaction will result in more homopolymer than grafted-copolymer. For this reason, it is beneficial to first covalently modify the surface of the cellulose with the initiator before attempting a grafting polymerization.

One of the most popular grafting methods in literature for cellulose modification has been with atom transfer radical polymerization (ATRP), in which a halogen-containing initiator is first immobilized on the surface of the cellulose [34]–[36], [41], [47]. During ATRP, a radical or active group is created with a redox reaction in the presence of a metal catalyst, resulting in a living-end reactive site attached to the cellulose from which the polymer chain will grow [47]. ATRP has gained a great deal of attention because it allows for extensive control over molecular weight and is compatible with a wide range of monomers [35]. However, drawbacks to ATRP are extreme sensitivity to oxygen, high cost and low efficiency [35], [47].

In addition to ATRP initiators, grafting of other forms of initiators, such as photoinitiators, have also been investigated to a lesser extent. UV is a convenient, low energy and safe means of initiating and controlling a radical polymerization reaction [36], [38]. Hong et al. used immobilized benzophenone to graft acrylamide from the surface of cotton fabrics to make them more hydrophobic, antimicrobial and durable [38]. The authors successfully grafted poly(acrylamide) and concluded that the grafting rate was increased with higher concentrations of immobilized initiator and longer exposure time under UV light.

Biyani et al. also used immobilized benzophenone in order to encourage CNC participation in crosslinking with an ethylene oxide/epichlorohydrin copolymer matrix [45]. The resulting properties after UV exposure included increased stiffness, reduced swelling from moisture and

increased shape memory. For 10% w/w and 20% w/w CNC-filled composites, the tensile storage modulus increased from 222 MPa and 407 MPa to 293 MPa and 508 MPa, respectively, after exposure to UV. In this study, the initiators were activated after the composite was formed in order to improve the interface between the phases through covalent cross-linking. However, this technique would not improve the initial dispersion of the CNCs within the hydrophobic matrix when the composite was created because there was no modification to improve the phase compatibility.

The purpose of this project was to modify CNCs with a photoinitiator that would facilitate the grafting of the polymer PMMA onto the crystals' surfaces to improve matrix-reinforcement interface in nanocomposites. This literature review indicated that limited research has been done for the grafting of CNCs compared to other forms of cellulose. Of the CNC grafting modifications that have been investigated, few have taken advantage of the possibility of immobilized UV-activated photoinitiators.

2.2 Poly(methyl methacrylate)

2.2.2 Composites and grafted polymers with PMMA

PMMA is commonly used for copolymerization and grafting in order to alter the surface properties of nanoparticles including carbon black, carbon nanotubes, nanocellulose and chitosan [13], [29]–[31], [49]. PMMA was bonded to carbon nanotubes to improve the dispersion and solubility of the nanoparticles [13]. The polymer was graphed to sodium alginate and cellulose acetate in order to

modify the characteristics of the materials [40], [50]. Grafted copolymers of chitosan and PMMA (chitosan-g-PMMA) resulted in biodegradable copolymer films, which improved the solubility of chitosan in nonprotonating solvents [51]. Chitosan-g-PMMA copolymers have been proposed as potential drug delivery materials [15]. PMMA has also been grafted onto bacterial polysaccharides through microwave-activated radical reactions in an aqueous suspension [52]. The resulting polysaccharides were more hydrophobic and crystalline and had promising characteristics for catalytic applications.

2.2.3 Photopolymerization of PMMA

Traditionally, PMMA was synthesized using thermally activated peroxide radical initiators. The use of higher temperatures (above 50^{o}C) resulted in faster reactions, however this could be very dangerous with exothermic polymerizations because the temperatures could increase very rapidly and uncontrolledly. Lower temperature conditions result in reactions that take hours to complete. Thermally activated reactions also allow for very little control over the conditions of the system once the reactions start [2]. Fortunately, PMMA synthesis is not limited to heat activated peroxides and the polymerization of MMA can be performed with a variety of techniques.

ATRP has gained attention as a method with narrow polydispersity and moderate reaction rates [53]. After Matyzaszewski et al. discovered the technique of ATRP, he successfully applied it to the production of PMMA in 1995 [54]. Since the development of ATRP, PMMA has been one of the most studied systems with this technique [53]. Guan et al. found that the rate of reaction with ATRP can be increased with the exposure to visible light during PMMA polymerization [55].

However, ATRP is an expensive reaction that is not readily adapted to industrial applications [56]. It is also highly oxygen sensitive and requires toxic, halogenated initiators [56].

Other researchers have investigated the potential of using light-initiated radical polymerization, specifically in the ultra-violet region of the spectrum. Charlot et al. was able to polymerize PMMA using several systems of photoinitiating compounds [2]. The most successful initiating system was a Type II system with isopropyl thioxanthone (ITX) and ethyl 4-(dimethylamino)benzoate (EDB). Altering the amount of ITX made it possible to tailor the molecular weight of the final polymer by controlling the number of radicals generated. UV-initiation makes it possible to tightly regulate the reaction time and the location of exposure during the polymerization. Light curing could be useful when grafting with a material that is sensitive to heat degradation and with polymerizations that are extremely exothermic. The use of UV-light curing makes it possible to pursue initiators that are less toxic than those used in ATRP while still allowing for a high degree of control.

CHAPTER 3: MATERIALS AND METHODS

3.1 Materials

All chemicals were ordered from Sigma Aldrich and used as received unless otherwise specified. The sulfonated cellulose nanocrystals (s.CNCs) (10.7% aqueous) were provided by Forest Products Laboratory from softwood hydrolyzed in sulfuric acid and used as the starting material for any CNC modifications [57].

3.2 Modification of cellulose

3.2.1 Transfer of cellulose nanocrystals into acetone

Approximately 250 mL acetone was added to 100 g of 10.7% w/w aqueous s.CNCs (Forest Products Lab) in a 500 mL beaker and stirred until the solution no longer had a gel-like consistency. The solution was then transferred to 250 mL centrifuge vessels and spun at 3500 rpm for 20 minutes. The supernatant was discarded and the pellet resuspended in fresh acetone. This acetone rinse was repeated three times. After the final rinse, the solution was resuspended in about 200 mL of acetone and sonicated for 15 minutes to minimize agglomeration. The concentration of s.CNCs in acetone was measured using triplicates of percent solid measurements. To find percent solid, a small sample of the solution was weighted into a metal weighing dish and allowed to evaporate in the hood. The final dry weight was measured and the percent solid calculated [Eq. 3].

$$\%\ solid = \frac{mass\ \ of\ dry\ solid\ (g)}{mass\ of\ solution\ before\ drying\ (g)} \times 100\% \qquad \text{[Eq. 3]}$$

3.2.2 Synthesis of anhydride initiator starting material

In a 150 mL round bottom flask, trimethylamine (2.5 mL, 18 mmol) was added dropwise to a 0.5 M solution of 4-(dimethylamino)benzoic acid (3.0 g, 18 mmol) in THF while stirring at room temperature. To this solution, a 1.0 M solution of pivaloyl chloride (2.2 mL, 18 mmol) in THF was added dropwise. The reaction was stirred at room temperature for 1 hour. Filtration was used to isolate the protected anhydride product from the precipitated salt byproduct, followed by two

chilled acetone rinses. The excess THF and acetone were evaporated and the resulting solid was recrystallized in acetone. The product was characterized with FTIR, elemental analysis and NMR.

3.2.3 Optimization of reaction time for modification of cellulose with initiator

In a 250 mL round-bottom flask, 3 g of s.CNCs (6-8% solution in acetone) were mixed with the protected anhydride starting material (2 g, 5.2 mmol) and p-tolusulfonic acid monohydrate (PTSA) (0.0113 g, 0.06 mmol) at 55ºC. Samples of the reaction were taken at 15 minutes, 30 minutes, 1 hour, 2 hours, 4 hours and 6 hours. Each aliquot was centrifuged for 10 minutes at 3500 rpm. The supernatant was discarded and the product was resuspended in fresh acetone. This rinse step was repeated three times. Each time point was characterized with FTIR and elemental analysis for % weight total nitrogen (TN) and % weight total carbon (TC).

3.2.4 Modification of cellulose with initiator

In a 250 mL round bottom-flask, 4.5 g of s.CNCs (6-8% solution in acetone) were stirred with the protected anhydride of 4-(dimethylamino)benzoic acid (2 g, 8 mmol) and PTSA (0.0177 g, 0.09 mmol) at 55 ºC for 6 hours. The reaction was then centrifuged for 10 minutes at 3500 rpm. The supernatant was discarded and the product was resuspended in fresh acetone. The rinse step was repeated two more times. The rinsed pellet was resuspended in acetone to approximately 7% w/w modified CNCs and sonicated for 10 minutes. The final concentration was found using percent

solids. The modification of cellulose was confirmed and characterized using FTIR and elemental analysis.

3.2.5 Optimization of co-initiator ITX for grafting of PMMA to CNCs

In four 20 mL scintillation vials with stir bars, a 5% w/w solution of initiator-modified CNCs in acetone (approximately 0.4 g initiator-modified CNC) was mixed with MMA (10 g, 10.6 mL). To each vial was added a different concentration of ITX in percentages relative to the moles of initiator on the modified CNC: 0 g (0%), 0.0028 g (19%), 0.005 g (38%), 0.0125 g (97%). Each vial was stirred under a xenon/mercury UV lamp (Hamamatsu, Model E7536) for two hours. The reaction was then diluted with 40 mL acetone and centrifuged at 3500 rpm for 10 minutes. The supernatant was decanted and dried to isolate the homopolymer produced in each reaction. The pellet was rinsed three more times. The pellets were each dried and weighted to monitor the change in weight of the grafted CNC.

3.2.6 Grafting of PMMA to CNCs

In a 20 mL scintillation vial containing a stir bar, a 7.5% w/w solution of initiator-modified CNCs in acetone (approximately 0.5 g CNCs), ITX (5mg, 0.02 mmol) and MMA (9g, 9.6 mL) were combined. The vial was sealed and placed on a stir plate under a xenon/mercury UV lamp (Hamamatsu Model E7536) [Figure 6].

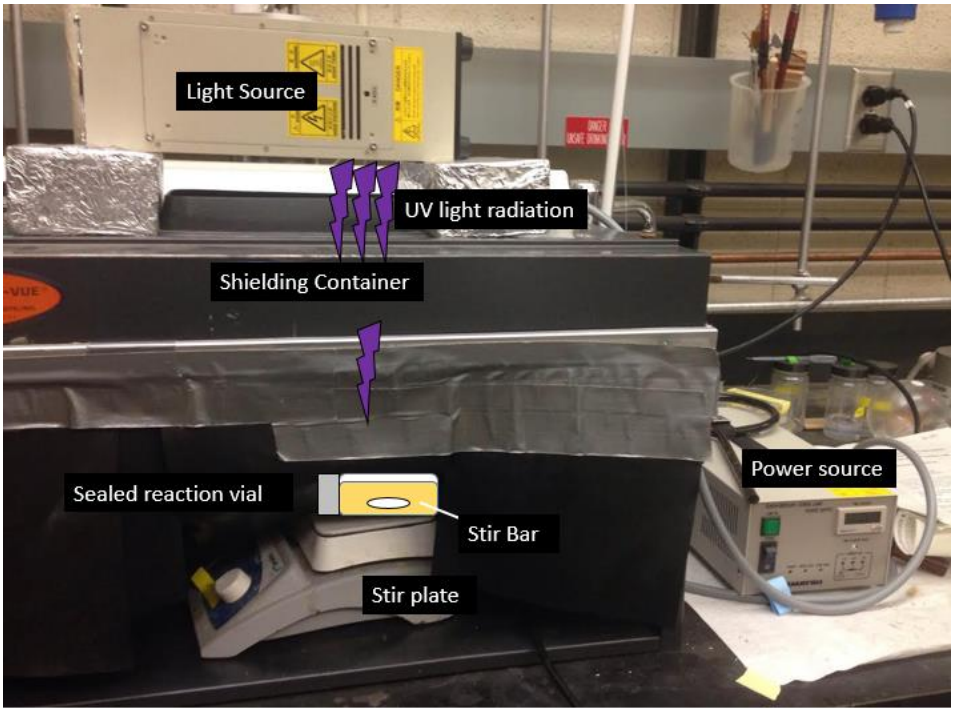

Figure 6: Set-up for photopolymerized grafting of PMMA onto initiator-modified CNC

The reaction was allowed to run for 5 hours. The mixture was centrifuged for 2 hours at 3500 rpm and the supernatant was decanted. This supernatant was evaporated in the hood to isolate the homopolymer from the acetone and unreacted monomer. The pellet was resuspended in fresh acetone and left overnight to dissolve any adsorbed homopolymer. A small portion of the PMMA-grafted CNCs (CNC-g-PMMA) was dried and characterized using FTIR and elemental analysis.

3.2.7 Ungrafting PMMA from CNC-g-PMMA

A 10 mL aliquot of acetone-rinsed CNC-g-PMMA pellet (approximately 0.4 CNC-g-PMMA) was mixed with 40 mL RODI H_2O and centrifuged for 30 minutes at 3500 rpm. The pellet was resuspended in 20 mL of 0.05 M citrate buffer (pH 4.8) in a 30 mL vial with a cap [58]. To the vial, 0.4 mL of *Trichoderma reesei* cellulase was added. The solution was incubated at 50^{o}C for 2

days. After the incubation period, the solution was boiled for 10 minutes to denature the enzyme. The solution was then centrifuged for 4 hours and the supernatant was decanted. The pellet was resuspended in 50 mL of fresh acetone and allowed to sit overnight to dissolve the ungrafted PMMA. The mixture was centrifuged again for 4 hours and the supernatant was decanted and allowed to evaporate to isolate any ungrafted PMMA. The acetone rinse was repeated two more times. The resulting PMMA solid from the supernatant was characterized with FTIR, NMR and mass spectroscopy.

3.3 Making CNC/PMMA and CNC-g-PMMA/PMMA Composites

Composites were made in 20 mL scintillation vials by dissolving approximately 0.5 g PMMA (mw 75000, Sigma Aldrich) in about 10 mL acetone. Two PMMA films were made by casting the PMMA solution into an aluminum weighing dish (100 mm diameter) without adding any cellulose. CNC/PMMA composites were made by adding the appropriate amount of CNC transferred into acetone to get 1% w/w, 5% w/w, 10% w/w and 15% w/w CNC. CNC-g-PMMA composites were made with this same method, using CNC that had been grafted with PMMA. Previous experiments showed that the grafting procedure produced CNC-g-PMMA with about 50% w/w CNC. This assumption was used to calculate the amount of CNC-g-PMMA to add to make composites of 1% w/w, 5% w/w, 10% w/w and 15% w/w CNC with two separate batches of grafted CNC. The actual amount of CNC in CNC-g-PMMA was later determined with elemental analysis and the true amount of CNC was determined in the composites as shown in Table 4.

Table 4. Predicted and Measured % w/w CNC in CNC-g-PMMA/PMMA composites

Batch	**% w/w CNC in CNC-g-PMMA determined with EA**	**% w/w CNC in CNC-g-PMMA/PMMA composite**	
		Predicted	Actual
A	62.4%	1%	0.7%
		5%	3.6%
		10%	7.2%
		15%	10.9%
B	65.5%	1%	5.4%
		5%	3.8%
		10%	6.9%
		15%	10.4%

All CNC/PMMA and CNC-g-PMMA/PMMA composites were stirred overnight. A small sample was taken from each solution and dropped onto a polished glass microscope slide before casting the remaining solutions into aluminum weighing dishes. Both the samples on the slides and in the dishes were evaporated under the hood until solvent was removed.

The films were then wrapped in aluminum foil and pressed between two metal plates in a heated press (Carver, Standard Auto Benchtop Press) at 318 kg and 135^{o}C for 20 minutes. If bubbles resulted from the pressing, the films were crushed into a powder and repressed until no bubbles remained. The films were prepared for mechanical testing by cutting them into dog bone shapes with a CO_2 laser (60 W, 2.0 lense, BLS 4.6 Universal Laser System) with settings for continuous cast PMMA (60.0% power, 66% speed, 500 PPI). The dog bones were made with the straight length of 16.8 mm and a width of 3.5 mm. The thicknesses of all the samples ranged from

0.2 mm to 0.97 mm and were measured with a horseshoe digital micrometer. For two samples (15% CNC-g-PMMA composites for both Batch A and B), the dimensions were smaller, 2.3 mm wide and 11.3 mm long, due to the limited amount of CNC-g-PMMA available for these batches. For each material, 3-4 dog bones were made. The composites on the microscope slides were observed under the optical microscope for evidence of agglomeration in the different composites.

3.4 Characterization techniques

3.4.1 Attenuated Total Reflectance Fourier Transform Infrared (ATR-FTIR) spectroscopy

All FTIR spectra were taken from dried and powdered samples with a Thermo Fischer Nicolet iS50 FT-IR spectrometer using attenuated total reflectance (ATR) technique. The ATR tip (1mm) and the surface of the instrument were cleaned with methanol and cellulose-fiber tissue (Kimwipes) between each analysis. For each spectrum, 16 scans at spectral resolution of 4 cm^{-1} were taken. Spectra were processed with Thermo Scientific OMNIC Spectra Software with ATR correction and manual baseline correction (7 conserved points).

3.4.2 Nuclear Magnetic Resonance (NMR) Spectroscopy

All samples were dissolved in acetone-d6 and their spectra were taken in the Bruker 700 MHz Avance III Spectrometer. The spectra were analyzed using Topspin 2.1 software.

3.4.3 Elemental Analysis

The weight percentages of total carbon (TC) and total nitrogen (TN) were found through combustion in a Perkin Elmer 2400 CHN Elemental Analyzer. Samples of 15-23 mg and 0.5-1 mg for TN and TC, respectively, were weighed and enclosed in tin capsules (4 mm x 3.2 mm; Elemental Microanalysis).

3.4.4 Differential Scanning Calorimetry (DSC)

DSC was performed with TA Instruments Q2000 DSC. CNC and CNC-g-PMMA samples were dried from acetone for 2 days and powdered in preparation for DSC. PMMA (Sigma Aldrich, mw 75000) was used as purchased in bead form. In T-Zero pans, 13 mg of the samples were tested at a ramping rate of 10^{o}C/min from 20^{o}C to 200^{o}C under N_2 atmosphere. The T_g for each material was calculated using the TA Universal Analysis software.

3.4.5 Thermogravimetric Analysis (TGA)

TGA was carried out with TA Instruments Q500 Thermoanalyzer from room temperature to 550^{o}C at heat rate of 10^{o}C/min under N_2. All samples were prepared with the same method as the DSC samples.

3.4.6 Stress-Strain Mechanical Testing

The PMMA and composite dog bones were broken with a 100 N cell on an Instron 5582 with the custom setup shown in Figure 7.

Figure 7. Instron 5582 custom 100 N load cell

The samples were tested until they broke or until reaching the maximum load of the load cell. The stress and strain of the samples were used to calculate Young's modulus for each composite in Excel.

3.4.7 Mass Spectroscopy

The samples of ungrafted PMMA from the CNC-g-PMMA were dissolved in acetone and submitted for analysis. They were run on a JEOL Mass Spectrometer using a FAB+ ionization mode in glycerol and NBA matrices.

3.4.8 Transmission Electron Microscopy (TEM)

All TEM samples were transferred to copper 400 mesh grids from dilute water solutions (s.CNCs and initiator-modified CNC) or dilute acetone solutions (CNC-g-PMMA) for 2 minutes and stained for 1 minute using 1% phosphotungstic acid (PTA). Grids were imaged using FEI Titan 80-200 STEM with Spot Size 3 and 200 V.

This material is based upon work supported by the National Science Foundation via the Major Research Instrument (MRI) Program under Grant No. 1040588. We also acknowledge the Murdock Charitable Trust and the Oregon Nanoscience and Microtechnologies Institute (ONAMI) for their financial contribution towards the OSU Titan TEM.

CHAPTER 4: RESULTS AND DISCUSSION

The purpose of this project was to modify the surface of CNCs to improve matrix-reinforcement interface and nanocrystal dispersion in CNC/polymer composites. This modification involved the immobilization of a UV light-initiator and the photopolymerized grafting of PMMA onto the nanocrystals. The optical clarity and mechanical properties of CNC-g-PMMA/PMMA composites were compared to those of ungrafted s.CNC/PMMA composites and neat PMMA to demonstrate any improvements from the CNCs modification.

4.1 Modification of cellulose

Initial weight change experiments indicated that simply adding CNCs to a polymerization reaction was not an efficient means of achieving a polymer graft, often resulting in mostly homopolymer. To ensure that the PMMA chain covalently grafted to the surfaces of the CNCs, it was decided that a UV-activated initiator should be immobilized on the nanocrystals. This would result in a "grafting from" polymerization where the polymer chain would grow from the active radical species on the CNCs surface. It was expected that, while there would still be competing polymerization of PMMA homopolymer, this reaction would not interfere with the successful polymer grafting reaction.

Several initiator systems were considered when deciding which molecule to immobilize onto the CNCs, including derivatives of benzophenone and 2,2-Dimethoxy-1,2-diphenylethane-1-one (Irgacure 651, Sigma Aldrich). However, Charlot et al. demonstrated that the Type II co-initiating system EDB and ITX is ideal for UV-polymerized PMMA [2] [Figure 8].

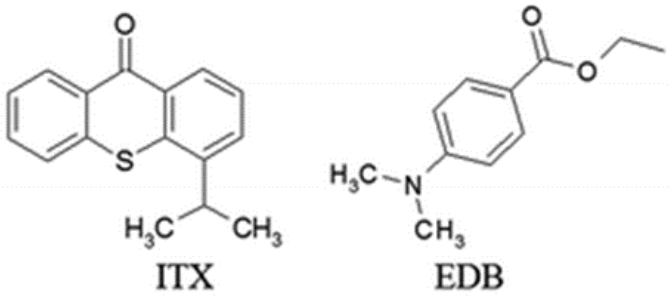

Figure 8. Co-initiating system for UV polymerization of PMMA [2]

When exposed to UV light, ITX is excited to a triplet-triplet state. One of the methyl groups adjacent to the tertiary amine on EDB then acts as a proton donor [18]. This quenches the triplet

state of ITX and creates two radical species: a ketyl radical ($ITXH^{\bullet}$) and an aminoalkyl radical ($EDB_{-H}^{\bullet}$). Since aminoalkyl radicals are known to react with double bonds much faster than ketyl radicals the deprotonated $EDB_{-H}^{\bullet}$ is the initiating radical for the polymerization [Figure 9] [2].

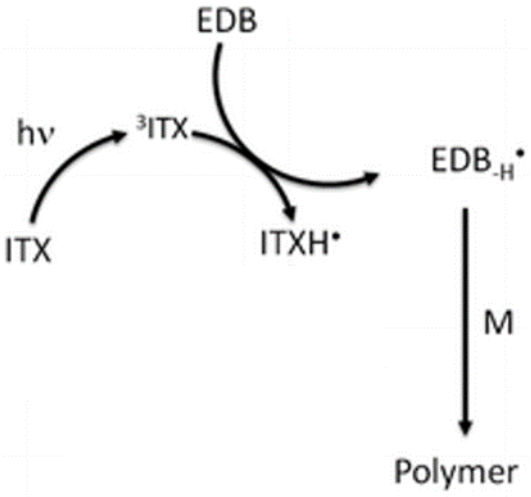

Figure 9. Photoinitiation mechanism of EDB-ITX initiator system. Image modified from [2].

While this mechanism has been well studied for free EDB and ITX compounds, it is unsure if the exact same pathways would be followed once the EDB was immobilized onto the surface of the cellulose. The proton could be scavenged from other sources, such as the surface of the cellulose itself causing the polymer chains to grow in locations other than the immobilized EDB initiator.

Another benefit of using this initiator system was that the structure of EDB was convenient to modify and attach to cellulose using the reactive C6 primary hydroxide [Figure 10].

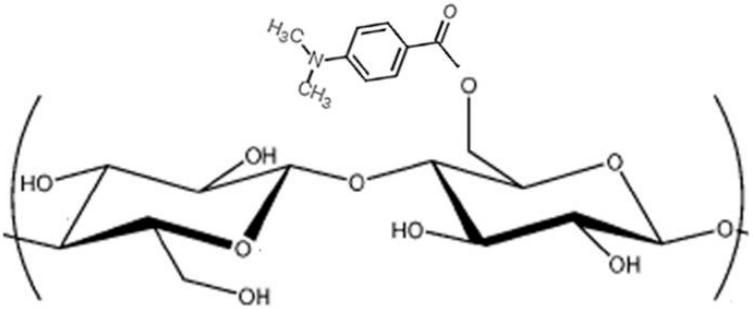

Figure 10. Modified cellulose with EDB-inspired initiator. Image modified from [5].

To accomplish this reaction, an anhydride was first made as the starting material to attach to the surface of the s.CNCs. A modified procedure adapted from Hong et al. converted 4-(dimethylamino)benzoic acid into an anhydride with a bulky tert-butyl group on the anhydride's opposite end [59] [Figure 11a]. This anhydride then reacted with the primary hydroxyl group on the cellulose to form an ester [Figure 11b]. The bulky tert-butyl group ensured the regioselective addition of the initiator side of the asymmetric anhydride [59].

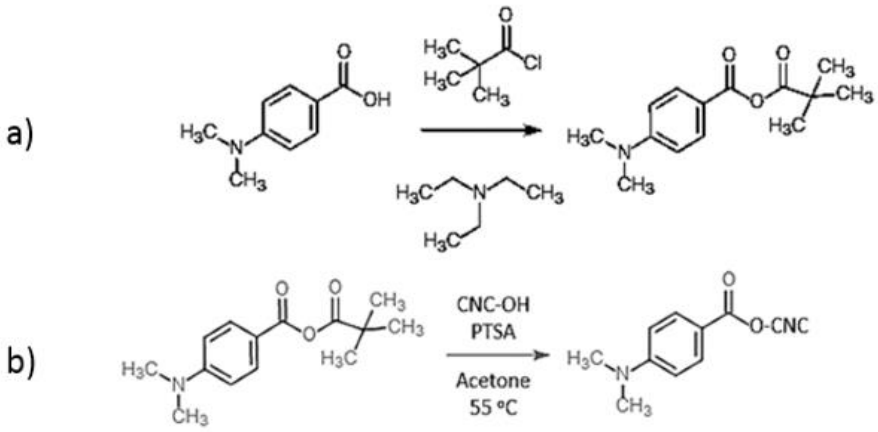

Figure 11. Preparation and immobilization of EDB-inspired initiator to CNC (a) The conversion of 4-(dimethylamino)benzoic acid to protected anhydride with bulky end-group (b) Grafting of initiator to CNC through the C6 hydroxyl group (CNC-OH)

4.1.1 Preparation of initiator to attach to CNC surface

The synthesis of the anhydride, shown in Figure 11a, was confirmed using ATR-FTIR, NMR and elemental analysis. The ATR-FTIR spectra indicate a definitive change between the starting material and the product [Figure 12].

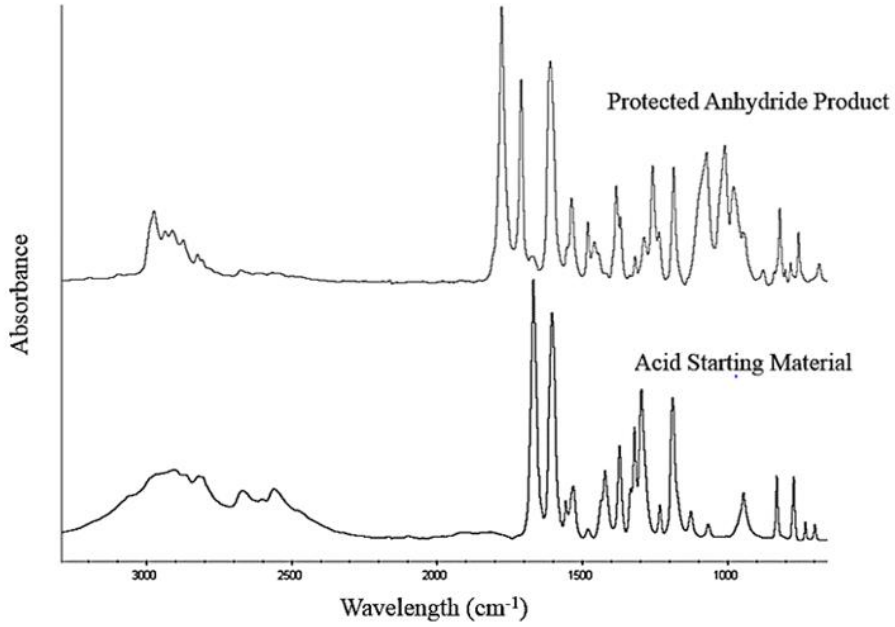

Figure 12. ATR-FTIR spectra of 4-(dimethylamino)benzoic acid and protected anhydride product

The spectrum of the starting material has the characteristic asymmetric O-H stretch broad peak around 2900 cm^{-1} of a carboxylic acid, which is notably absent from the resulting anhydride product. The product also has an unsaturated symmetric C=O stretch (1778 cm^{-1}) and unsaturated symmetric C=O stretch (1710 cm^{-1}) peaks that are typical of anhydrides and were not present in the acid starting material spectra [60].

NMR was also used to confirm the structure of the starting material and final product of the reaction [Figures 13 and 14]. In Figure 13, the NMR spectrum of the acid starting material shows the expected aromatic protons at 7.9 ppm and 6.7 ppm and six protons on the methyl groups attached to the tertiary amine at 3.0 ppm. In Figure 14, the final product shows the same aromatic and methyl protons with the addition of nine protons at 1.3 ppm from the tert-butyl group.

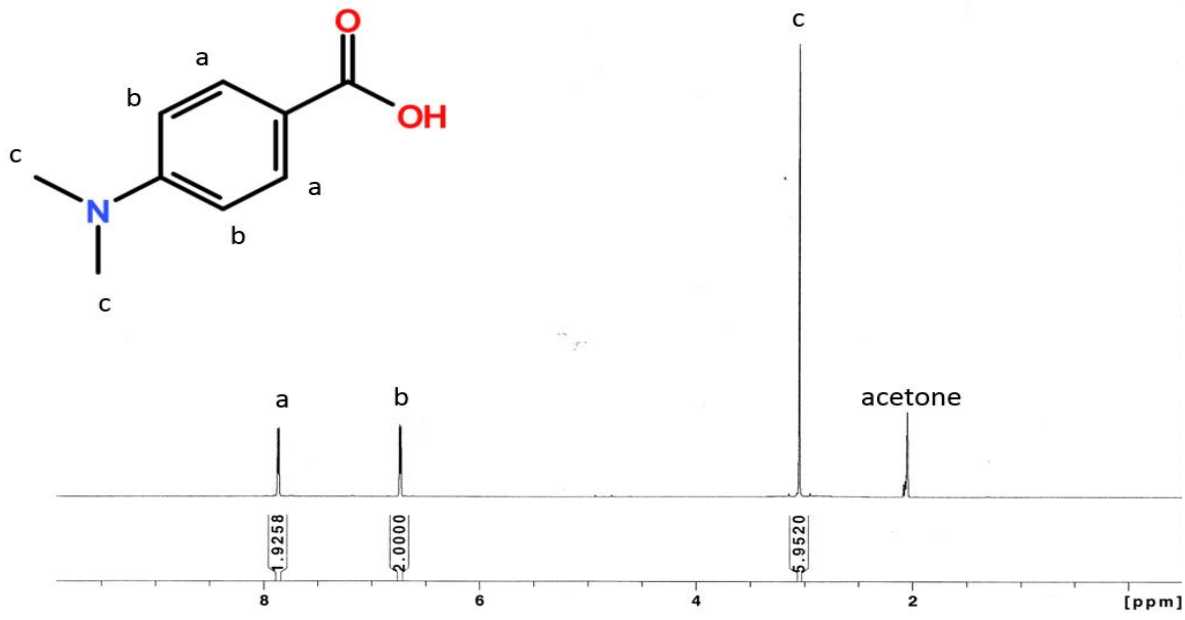

Figure 13. NMR spectra of starting material 4-(dimethylamino)benzoic acid with assigned peaks

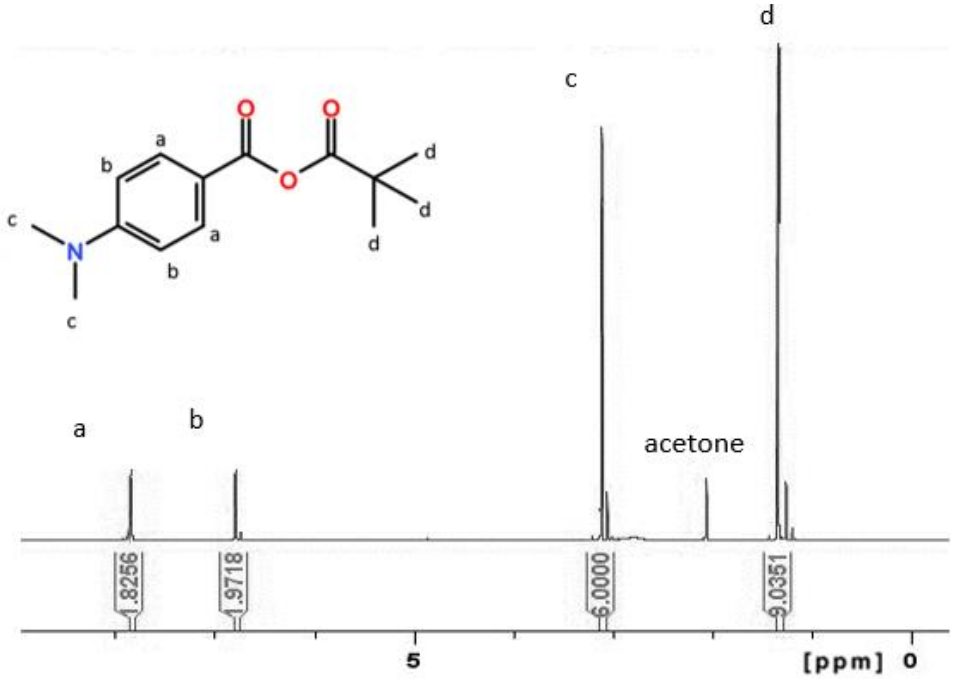

Figure 14. NMR spectra of protected anhydride product with bulky tert-butyl end group with assigned peaks

Elemental analysis further confirmed the structure and purity of the product anhydride. With the molecular formula of $C_{13}H_{19}O_3N$, the TN should be 5.9%. Elemental analysis measured the TN to be 5.93 ± 0.07%, demonstrating that the product was pure and that the presence of a single nitrogen was detectable in this compound. This technique was later used to track and quantify the amount of initiator attached to CNCs.

4.1.2 Initiator graft to CNCs

The successfully prepared anhydride was then bonded to the surface of the CNCs by reacting with the C6 primary hydroxide [Figure 11b]. Because of the nonpolar nature of the anhydride and the need for a solvent system compatible with MMA and PMMA, the CNCs were transferred to acetone. When transferred from water to acetone, the suspension changed from translucent blue to cloudy white. This raised concerns about the agglomeration of the CNCs in the new solvent. However, the modified CNCs in acetone still formed a clear film when dried, which indicates that the nanocrystals were not irreversibly agglomerated and were still nano-sized enough to maintain their characteristic transparency [Figure 15].

Figure 15. Dried film of modified CNC from acetone and unmodified CNC from water

Images taken with TEM of the modified CNC also show comparable levels of nanoparticle dispersion as found with s.CNC that remained in water. It was expected that, with frequent sonication at every step, the CNC-g-PMMA would successfully resuspend in non-protonating solvents and composites.

The graft of the initiator to the surface of the CNC was confirmed first with ATR-FTIR after the CNCs were rinsed several times to remove any unattached compounds [Figure 16].

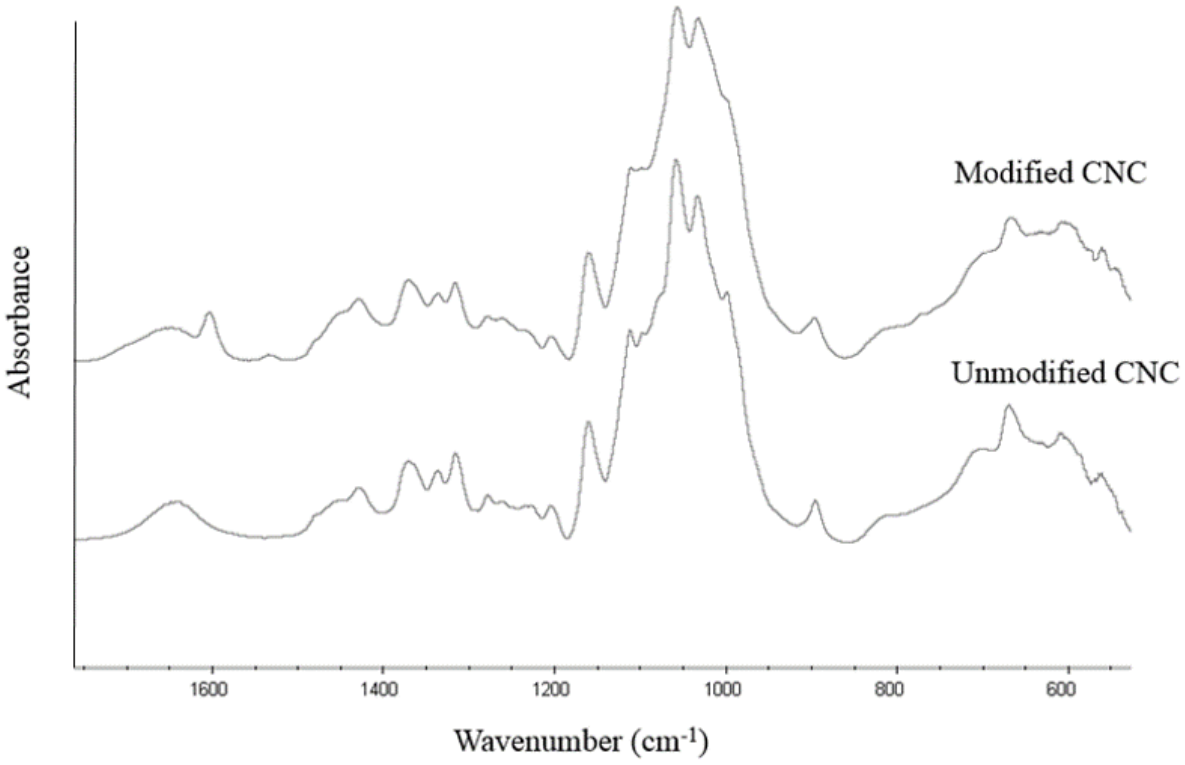

Figure 16. ATR-FTIR spectra of s.CNCs and CNCs modified with immobilized initiator

The spectrum of the modified CNCs showed the presence of a new peak at 1604 cm^{-1}, which could be the aromatic C=C stretch or C=O stretch from the attached initiator [60].

Elemental analysis was used to determine the concentration of grafted initiator onto the CNCs. Since there was a single nitrogen in each initiator, the TN of samples (g N/g sample) could

be converted to the amount of initiator grafted onto the CNC (mmol initiator/g sample). Samples of the reaction were taken at different time points to determine the possibility of controlling the concentration of initiator using reaction time [Figure 17].

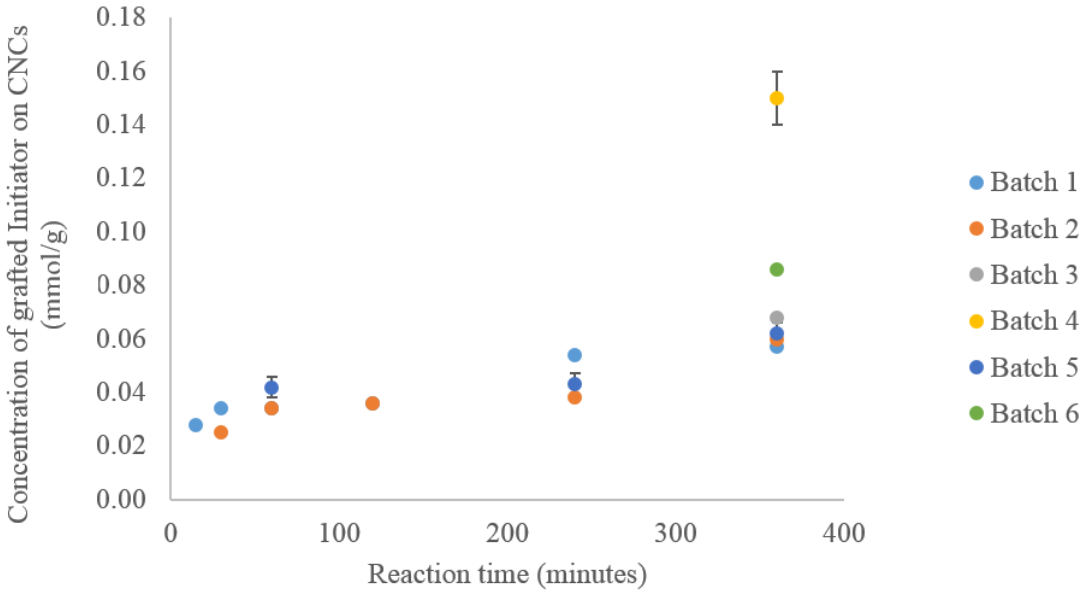

Figure 17. Time point experiment for CNC modification with immobilized initiator

This experiment showed that the concentration of the initiator could be controlled using time of the reaction. Due to the cost per sample with elemental analysis, triplicates were done for only select time points and batches to determine the variability within a sample. The average variation within a sample was 0.004 mmol/g, however could be as high as 0.03 mmol/g (Batch 4). While the concentrations of initiator seemed to be reproducible at specific time points, there was some variation between the different batches, as shown for the six hour time point in Figure 18. Batches 4 and 6 had concentrations considerably higher than the other batches. The average concentration at 6 hours was 0.08±0.03 mmol/g, however the average changes to 0.07±0.01 mmol/g when excluding the 0.15±0.03 mmol/g value of Batch 6.

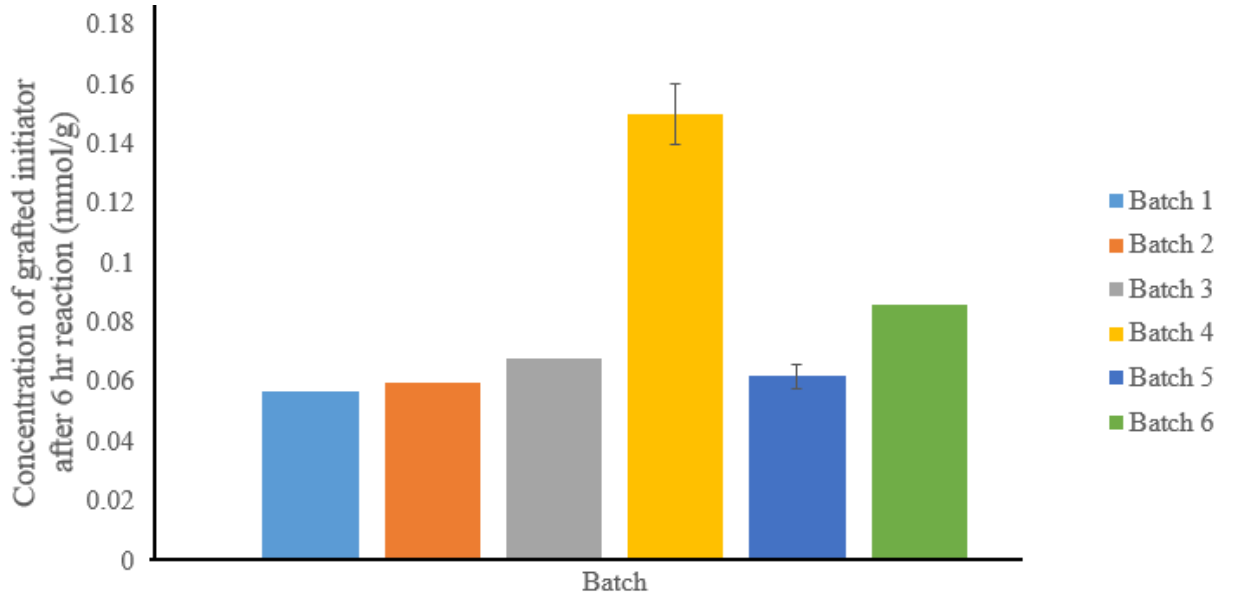

Figure 18. Grafted initiator concentration on CNC after 6 hour reaction for different batches

The high concentration of Batches 4 and 6 could be due to temperature fluctuations during the reaction and slight differences in reagent or catalyst amounts. It could also be related to the purity and quality of different batches of prepared anhydride. For most reactions, however, the concentration appears to be reproducible with the length of the reaction if all other factors are controlled.

4.1.3 Investigation of DMF as a solvent for CNC modification

While it was expected that suspending CNCs in acetone would not permanently agglomerate the nanoparticles, the cloudy appearance of the mixture was not considered ideal for maintaining individual nanocrystals. For this reason, other solvents were investigated as alternatives. DMF was identified a promising candidate because it both dissolved PMMA and dispersed CNCs well. CNCs were transferred into DMF with the same procedure used to transfer CNCs into acetone,

with the additional step of rotary evaporation under pressure to remove any remaining water. Initially, the initiator modification performed in DMF seemed promising. Figure 19 shows that the concentration of initiator immobilized onto CNCs in DMF was more than twice has high than the CNCs modified in acetone.

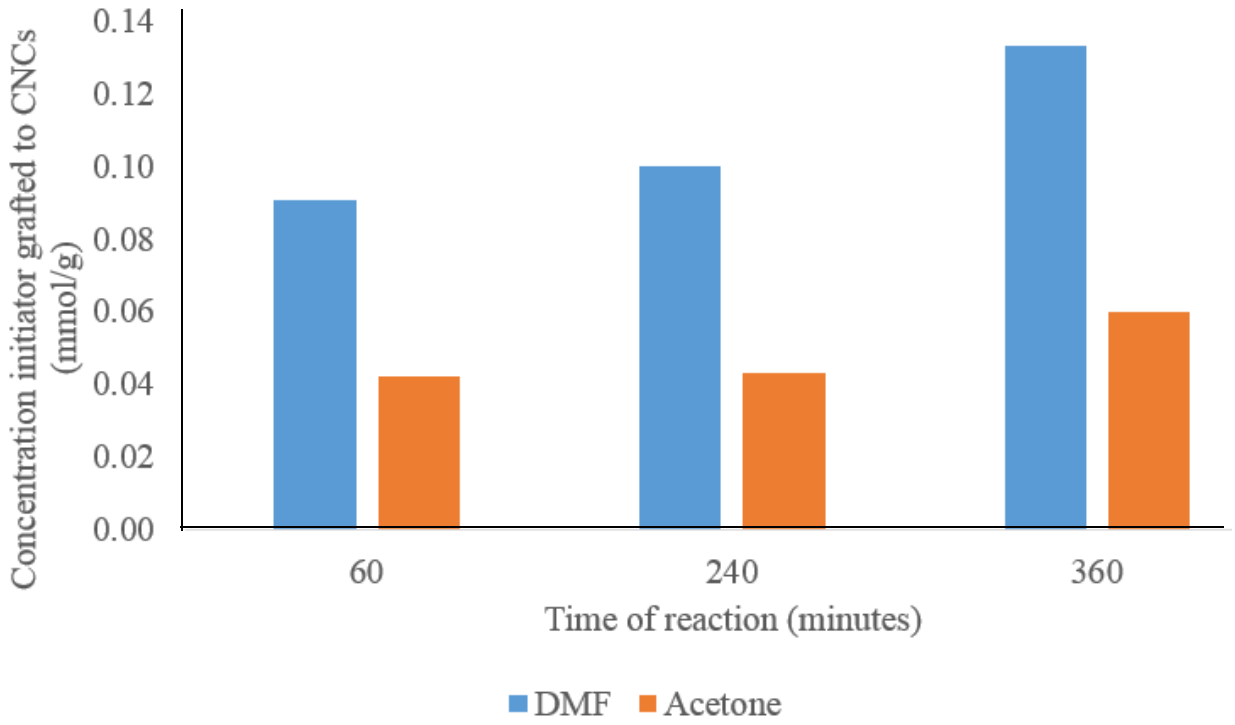

Figure 19. Comparison of initiator graft concentrations on CNCs from modification reactions in DMF and acetone

This could be because CNCs are better dispersed in DMF than in acetone, which reduces agglomeration and increases the available surface area that can react with the anhydride. However, it could also have been because the CNCs were too well dispersed in DMF, making it difficult to clean the modified CNCs of unreacted initiator. Since the CNCs were not very well suspended in acetone, it was convenient to centrifuge and wash the nanocrystals after the modification reaction. It was difficult to centrifuge and pellet the CNCs from DMF and so it is possible that the elemental analysis of CNCs modified in DMF measured a falsely high concentration of immobilized initiator.

Removing water completely from the DMF solvent after transferring the CNCs from water also proved to be a time-consuming processing barrier. Since DMF is extremely miscible with water, the water was never completely removed even after several centrifuge transfer steps and rotary evaporation. This issue caused problems when attempting to make solvent-cast s.CNC/PMMA composites from DMF [Figure 20]. Because water could not be completely removed, the hydrophobic polymer lost its optical clarity as the DMF solvent evaporated.

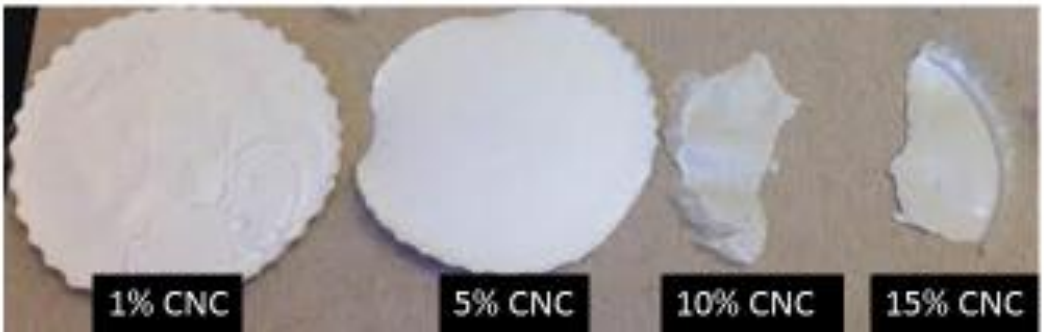

Figure 20. s.CNC/PMMA composites cast from DMF

An additional processing concern that arose with the use of DMF came from the greater relative toxicity of DMF compared to acetone. The process developed to modify the CNCs used large volumes of solvent and the procedure to make the CNC/PMMA composites involved the pressing of these films in a heated press that was not enclosed in a hood. It was also observed that the composites made from DMF remained noticeably “greasy” with the solvent for days after being cast. This indicated that the solvent was not easily removed from the composite and could alter the mechanical stiffness of the composite by acting as a plasticizer. The toxicity and persistence of the solvent in the composites made DMF an impractical solvent because these qualities would be undesirable when adapting this process to a manufacturing scale with consumer goods being produced. Overall, safety and efficiency led to the decision to continue with acetone as the solvent for the CNC modification.

4.2 Photopolymerized graft of PMMA from the CNC surface

After the characterization of the grafted initiator, the modified CNCs were used in a photoinitiated polymerization with the MMA. The modified CNCs were suspended in a mixture of acetone and monomer and exposed to UV light from a mercury/xenon lamp. The resulting CNC-g-PMMA was rinsed and separated from any unattached PMMA homopolymer and unreacted monomer. This product was then characterized with FTIR, elemental analysis, DSC and TGA.

The ATR-FTIR of the grafted CNCs shows a strong C=O stretch peak at 1725 cm^{-1}, which is characteristic of PMMA [Figure 21] [60].

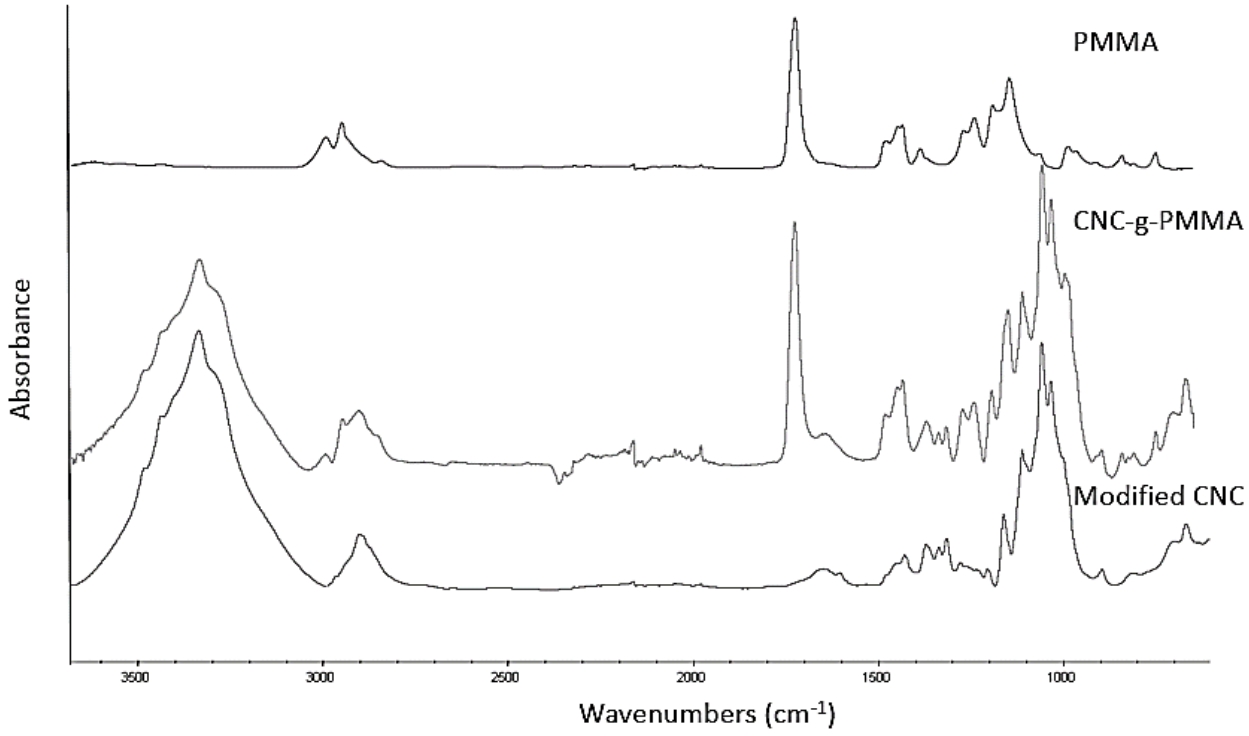

Figure 21. ATR-FTIR spectra of initiator modified CNC, CNC-g-PMMA and neat PMMA

The FTIR spectra of the grafted CNCs concluded that PMMA polymer chains had been covalently bonded to the cellulose crystals, confirming that the modified initiator adapted from EDB continued to function as a part of the Type II co-initiator system despite the alterations and immobilization to the surface of the nanocrystals. It should be noted that after the polymerization reaction, the CNC-g-PMMA turned from a white color to a yellowish tint, which could be due to the degradation of the cellulose under the elevated temperatures from the lamp used as a UV light source during the polymerization.

The grafting reaction was done with a range of ITX co-initiator to determine the effect of the initiator/co-initiator ratio on the amount of grafted PMMA on the cellulose. With ITX amounts of 0%, 19%, 38% and 97% mol/mol of the EDB-inspired grafted initiator, the weight gain due to PMMA grafting was found to be 122%, 180%, 155% and 157%, respectively. This indicated that, while the polymerization reaction could occur without the co-initiator, the grafting was more successful with the participation of ITX. It also demonstrated that a smaller ratio (19% mol/mol) of co-initiator to initiator resulted in greater amounts of grafted PMMA. The developed procedure used an ITX 55% mol/mol of EDB. This is not as low as the optimization experiment, however, on the scale of reactions performed smaller amounts of ITX were impractical to measure. Nevertheless, ITX concentration could be added in smaller amounts in future scaled-up batches or could be utilized as a means of controlling the degree of the PMMA graft without having to modify the concentration of the grafted EDB-like initiator.

4.2.1 Characterization of the CNC-g-PMMA

Once it was determined that PMMA could be successfully grafted onto the surface of modified CNCs, the nanocrystals were then characterized with TEM, elemental analysis, DSC and TGA. TEM was used to determine if the initiator modification and polymer grafting changed the shape, dimensions or dispersion of the nanocrystals compared to the s.CNCs [Figure 22].

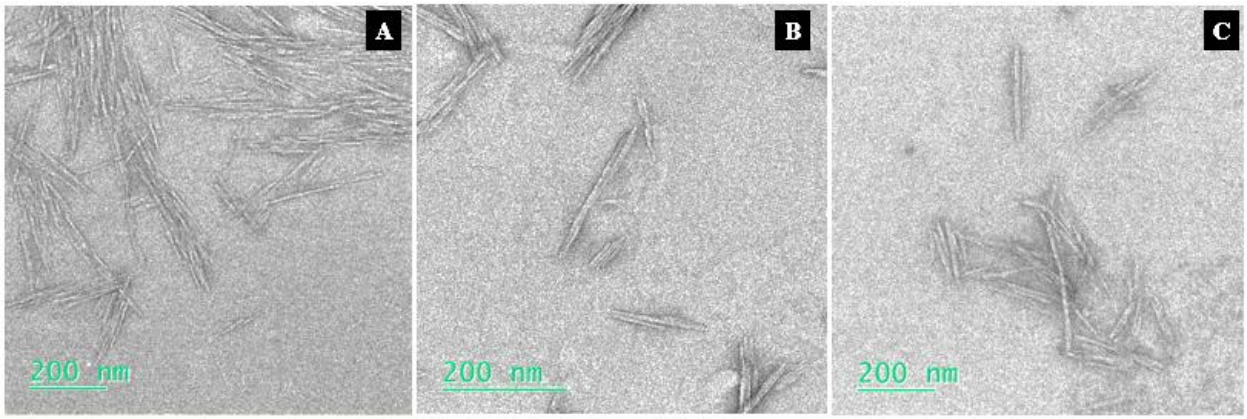

Figure 22. TEM images of (A) sulfonated CNC (B) initiator-modified CNC and (C) CNC-g-PMMA

By randomly sampling the dimensions of 20 nanocrystals from various areas of the copper TEM grids, the lengths and diameters of the s.CNC crystals, initiator-modified CNC and CNC-g-PMMA were measured. The results summarized in Table 5 suggest that there was no difference in length or diameter dimensions between the CNCs before and after the initiator modification.

Table 5. Dimensions of CNC with various modifications measured with TEM

Dimension	Sulfonated CNC (nm)	Initiator modified CNC (nm)	CNC-g-PMMA (nm)
Length	160 ± 30	160 ± 40	170 ± 50
Diameter	8 ± 2	8 ± 3	11 ± 3

This confirms that the PTSA catalyst did not degrade the CNCs during the 6 hours of the reaction. The CNC-g-PMMA appear to have slightly longer and wider dimensions than the ungrafted CNCs, which could be evidence of an added coating of attached polymer. However, the variation in these measurements is too large to confirm the significance in the different sizes. The PTA stain from the TEM preparation was unable to capture any visible evidence of grafted PMMA chains.

The extent of the PMMA graft on the CNCs was initially estimated by measuring the change in weight of the CNCs before and after the polymerization. These initial experiments indicated that the CNC-g-PMMA were between 50-65% grafted PMMA. Elemental analysis was then used to more precisely measure the amount of grafted PMMA by observing the change in TC. The fraction of grafted polymer could be calculated using Equation 4,

$$C_g = (1 - t)C_{m.} + tC_P \qquad \text{[Eq. 4]}$$

where C_g, C_m and C_p are the TC of the grafted CNC-g-PMMA, initiator modified CNC and PMMA, respectively, and t is the weight fraction of the grafted polymer [61]. For the two grafting reactions prepared to make CNC-g-PMMA/PMMA composites, the CNC-g-PMMA were 62.4% and 65.5% w/w PMMA. The PMMA polymer content of the grafted cellulose was consistent with the fact that, when compressed with a heated press, the CNC-g-PMMA powder molded into a translucent

film. The fact that grafted CNC was able to be molded suggests the grafted PMMA could be a high molecular weight.

The physical properties of the nanocrystals were investigated with TGA and DSC. The TGA of s.CNC, PMMA and CNC-g-PMMA were used to compare the thermal stability of the different materials [Figures 23 and 24]. The TGA of CNC-g-PMMA showed characteristics that blended those of the purchased PMMA and the s.CNC. CNCs begin to degrade at 218^{o}C, which is much lower than the temperature at which PMMA begins to degrade (295^{o}C). CNC-g-PMMA begins to degrade between these values at around 260^{o}C. This is most likely because the PMMA grafted onto the surface of the CNCs shield the cellulose at temperatures that would normally degrade it. In addition to different degradation temperatures, the temperature ranges over which the materials degrade are different. CNCs degrade over approximately 280^{o}C (218^{o}C to 500^{o}C). PMMA degrades over about 114^{o}C (295^{o}C to 409^{o}C). CNC-g-PMMA has a degradation range between these ranges of 175^{o}C (260^{o}C to 435^{o}C). Overall, the TGA of the different material indicate that the grafted CNC has a blend of the individual physical properties of CNC and PMMA.

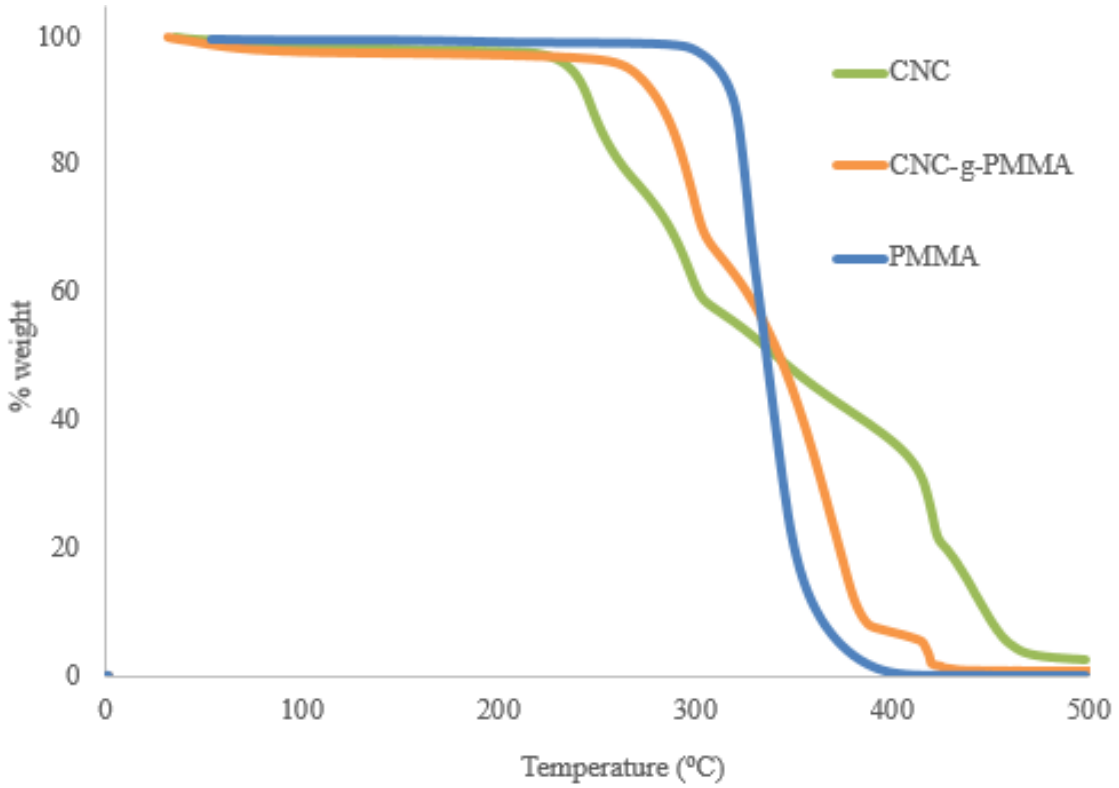

Figure 23. TGA of CNC, CNC-g-PMMA and PMMA

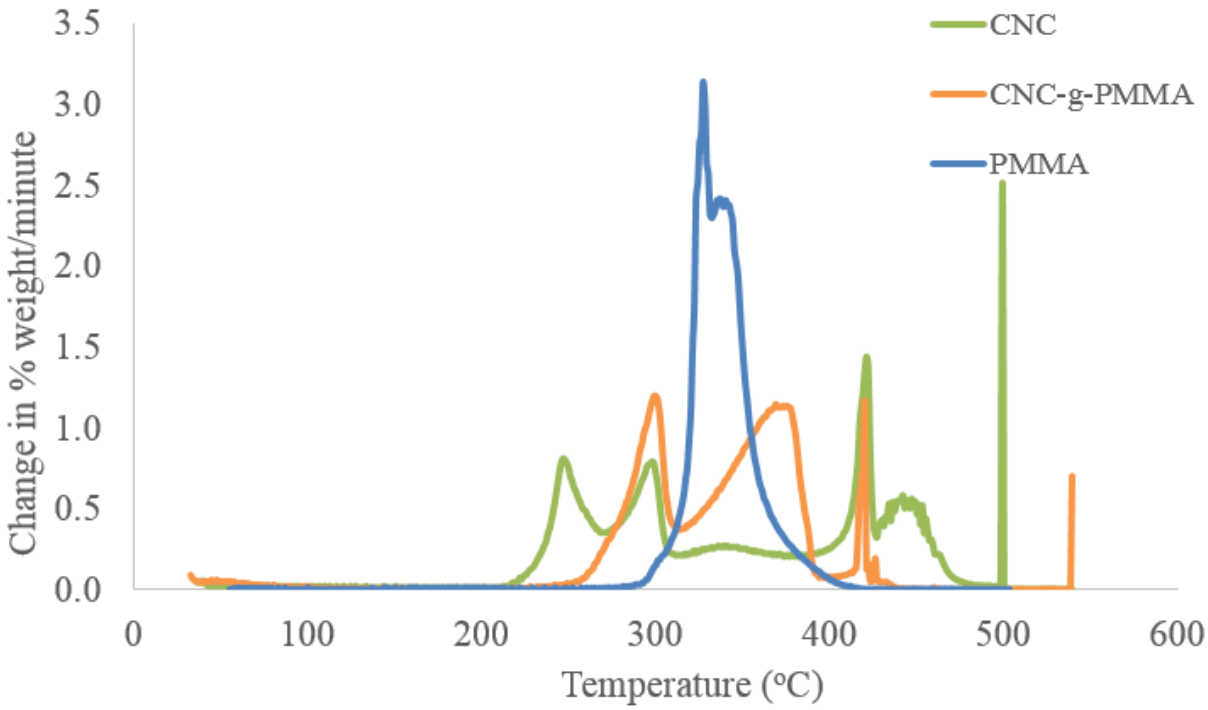

Figure 24. dTGA of CNC, CNC-g-PMMA and PMMA

DSC was also used to characterize physical differences between the s.CNC, PMMA and CNC-g-PMMA [Figure 25]. The T_g measured for the purchased PMMA (mw 75000 g/mol), 109°C, is close to literature values for the polymer [Table 3]. CNCs do not have an observed T_g.

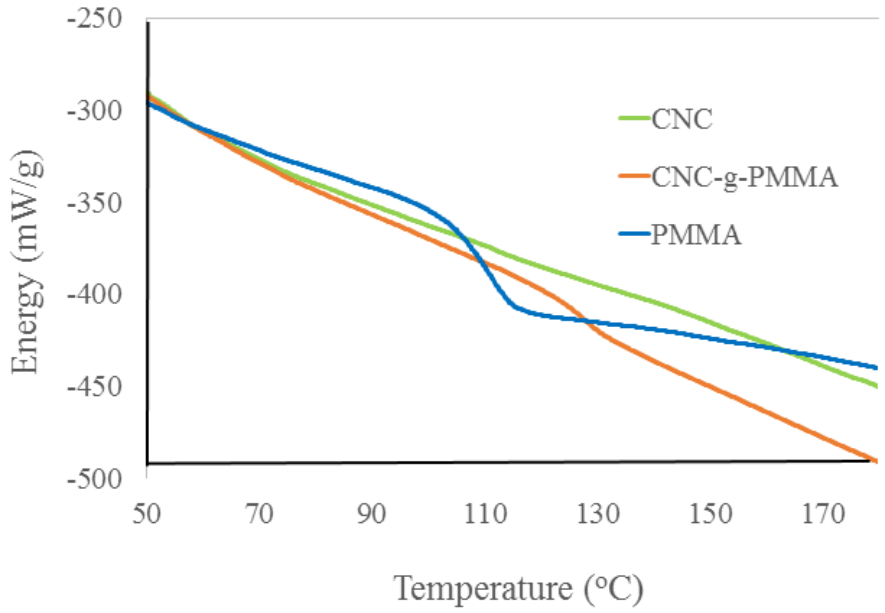

Figure 25. DSC of CNC, CNC-g-PMMA and PMMA

As with the TGA properties, the DSC of the CNC-g-PMMA exhibited a hybrid of s.CNC and PMMA characteristics. Like PMMA, CNC-g-PMMA had a T_g; however, it is higher than that of PMMA alone, which suggests that the covalent bond is restricting the movement of the chain.

4.2.2 The effect of immobilized initiator concentration on amount of PMMA in CNC-g-PMMA

While mechanism of the EDB-ITX initiator system has been studied and is fairly well understood, the mechanism of the immobilized initiator is not expected to be exactly the same. It is possible that the polymer chains will grow from the aminoalkyl radical of the EDB-inspired initiator, or

protons could instead be pulled from the surface of the cellulose itself to create many more active radical sites than the grafted initiators themselves. An experiment was designed to determine whether or not chains grow from the initiators exclusively or if other radically active sites could form. One experiment (Experiment A) was simply a preliminary experiment to determine whether the amount of PMMA in CNC-g-PMMA could be measured with elemental analysis. The second experiment (Experiment B) used initiator-modified CNCs from 1 hour, 4 hours and 6 hours reaction times to attempt to change the concentration of initiator to see if the amount of bonded PMMA would vary with differences in initiator concentration. The third experiment (Experiment C) used modified CNCs with the same concentration of grafted initiator to determine how reproducible the amount of added PMMA could be between reactions. Experiment C was used to make the CNC-g-PMMA/PMMA composites to test for mechanical properties [Figure 26].

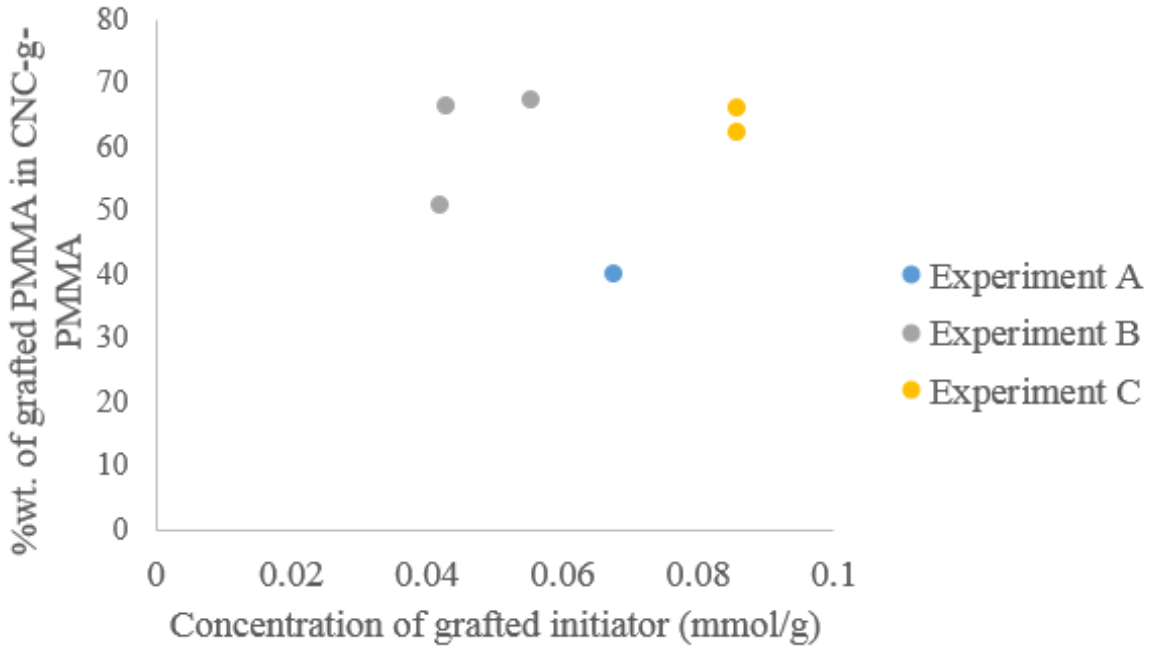

Figure 26. Different weight percent of grafted PMMA in PMMA-g-CNC for different immobilized initiator concentrations

The results summarized in Figure 26 do not provide evidence that the amount of PMMA grafted to the CNCs are dependent on the concentration of the initiator. Experiment B indicates that modified CNCs with different initiator concentrations can have a comparable amount of PMMA attached, while two modified CNCs with similar initiation concentrations have very different amounts of added PMMA. Additionally, Experiment A had an initiator concentration much higher than any concentration for Experiment B, however the amount of PMMA added was considerably lower than any amounts from Experiment B. It seems that the pathway of radical polymerization is not dependent on the concentration of the initiator. However, these variations could be due to other factors that are not yet controlled in the set-up for the photopolymerization. The current method used for the grafting reaction leaves the temperature of the reaction, mixing speed and intensity of the UV-light uncontrolled. This is not an ideal set-up and it could be improved using a set-up like the spinning disk reactor, which allows for a higher degree of control over these conditions. Grafting experiments done using such a set-up might better demonstrate how initiator concentration is affects the amount of grafted PMMA. Experiment C showed that the amount of grafted PMMA could potentially be reproducible given the same modified CNC batch is used.

4.2.3 Characterizing the PMMA grafted chains on the CNC-g-PMMA

The average molecular weight and molecular weight distribution of the grafted PMMA could have an enormous impact on how the polymer changes the interface of the CNCs within the polymer matrix. For this reason it is important to study the grafted PMMA. This was first attempted by

detaching the grafted PMMA from the surface of the nanocrystals using a cellulase enzyme. The PMMA was then rinsed from the CNC-g-PMMA with acetone and isolated to be investigated with FTIR and mass spectroscopy. FTIR was used to confirm that there was no cellulose still attached to the ungrafted PMMA. The sample was analyzed with mass spectroscopy to determine if a molecular weight of the ungrafted PMMA could be measured [Figures A1.1 and A2.2]. The resulting peaks are summarized in Table 6.

Table 6. Most prominent m/z peaks in mass spectroscopy of ungrafted PMMA

Matrix	**m/z of most prominent peaks from JOEL mass spectroscopy**
NBA	132, 166, 215, 284, 316, 391, 418, 474, 521, 660, 758. 791, 858
Glycerol	132, 184, 223, 284, 355, 392, 447, 483, 575, 615, 651, 742, 910

If the PMMA had been ungrafted and purified successfully, it would be expected to see chains with molecular weights of 100x, where x would be the number of repeating units within the chain. Molecular weights of (164+100x) would also be acceptable because it would mean that the initiator had been cleaved from the cellulose surface along with the chain. Ideally, these peaks would give the length of the chains and the average molecular weight of the polymer. FTIR of the cleaved PMMA indicated most of the CNCs had been removed. However, the mass spectroscopy did not provide peaks consistent with predicted values. The peaks found did not increase by any consistent increment and the peak values did not match with any of the possible combinations of PMMA repeat units, cellulose or initiator. It is possible that acid hydrolysis process used to make the s.CNC, the initiator and polymer grafting reactions and the cellulase digestion could have introduced additional ions or compounds that would dominate or confuse the mass spectrometry

data. It was also determined that this form of mass spectroscopy, while the only instrument available at the time for this project, was not ideal for the testing that was needed to find molecular weight. Matrix-assisted laser desorption/ionization (MALDI) would be the most appropriate method of mass spectroscopy for determining molecular weight for polymers. Other ideal methods of determining molecular weight would be size exclusion chromatography or solid state NMR through end-group analysis. The instruments for these tests were not available at the time of testing.

NMR end-group analysis works by recognizing that the chemical environment of the functional groups on the end of a polymer chain is slightly different from the environment within the chain. The ratio of the integrals of the peaks that belong to the end-group and those that belong to the groups within the chain can give the length of the polymer chain. While this experiment was not within the scope of this project, samples were prepared to be analyzed with this method. Experiment B from Chapter 4.2.2 was a reaction that took aliquots of the initiator-grafted CNC at three different reaction times (1 hour, 4 hour and 6 hour) with the expectation that this would provide a range of initiator concentrations. The initiator concentrations per gram of modified CNCs were measured to be 0.042 mmol/g, 0.043 mmol/g and 0.055 mmol/g respectively. Each group of modified CNCs were then grafted with PMMA under the same photoinitiation conditions, resulting in 50.8%, 66.1% and 67.2% w/w grafted PMMA. The CNC-g-PMMA from each reaction for Experiment B were then incubated with cellulase to remove the PMMA chains from the nanocrystals to submit for solid state NMR. The FTIR spectra in Figure 27 show that the majority of the cellulose was removed, although some cellulase remained with the 1-hour initiator modified CNCs. This impurity might impact the ability to detect end groups for analysis.

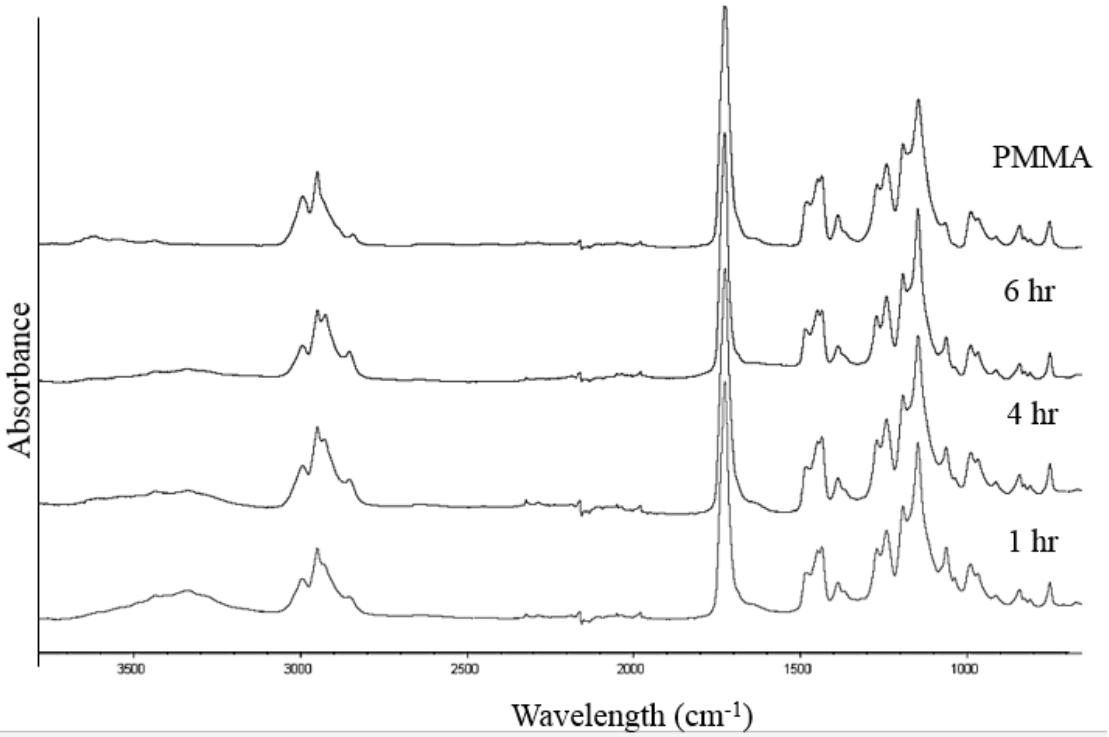

Figure 27. FTIR of ungrafted PMMA from CNC-g-PMMA made with CNC that had been modified

4.1 Properties of CNC-g-PMMA and s.CNC composites

PMMA composites made with CNCs and CNC-g-PMMA were compared optically and mechanically to neat PMMA samples. Literature reports that the addition of CNCs to polymers results in composites that have increased stiffness, although there is a maximum amount of CNCs that can be loaded before the nanoparticles begin to agglomerate and diminish the composite mechanical properties of the composite [45]. The final purpose of this project was to determine if CNC-g-PMMA made nanocomposites with improved interface compared to s.CNC composites and neat PMMA films. It was expected that, it the CNC-PMMA interface was improved with the

graft, then the mechanical and optical properties would be better for CNC-g-PMMA/PMMA composites than CNC/PMMA composites due to superior dispersion.

4.3.1 Optical clarity of CNC/PMMA and CNC-g-PMMA/PMMA composites

The optical clarity was monitored with neat PMMA, CNC/PMMA and CNC-g-PMMA/CNC films that were made by solvent casting drops onto microscope slides and observing them under a light microscope to look for signs of agglomeration or lack of transparency [Figure 28]. At about 1%, both CNC and CNC-g-PMMA composites seem to be comparable to the neat PMMA. However, as the amount of reinforcement increases, the samples became less transparent and more roughly textured under the microscope. It is unclear if the change is direct evidence of agglomeration or if it is from voids left from the acetone evaporation after being solvent cast, however the roughness does increase dramatically with the amount of reinforcement. The bubbles could have increased with the amount of nanoparticles because more solvent had to be added as the viscosity increases with the amount of nanofillers in the composite.

It was not possible to use samples that had been pressed in the heated press to eliminate bubbles because of the added surface roughness from the foil and the contaminants introduced during the melting step. No additional information about the agglomeration could be extracted using polarized light because the PMMA itself was birefringent. From the optical images taken with this method, there is no definitive indication that the CNC-g-PMMA/PMMA composites had better optical clarity than CNC/PMMA.

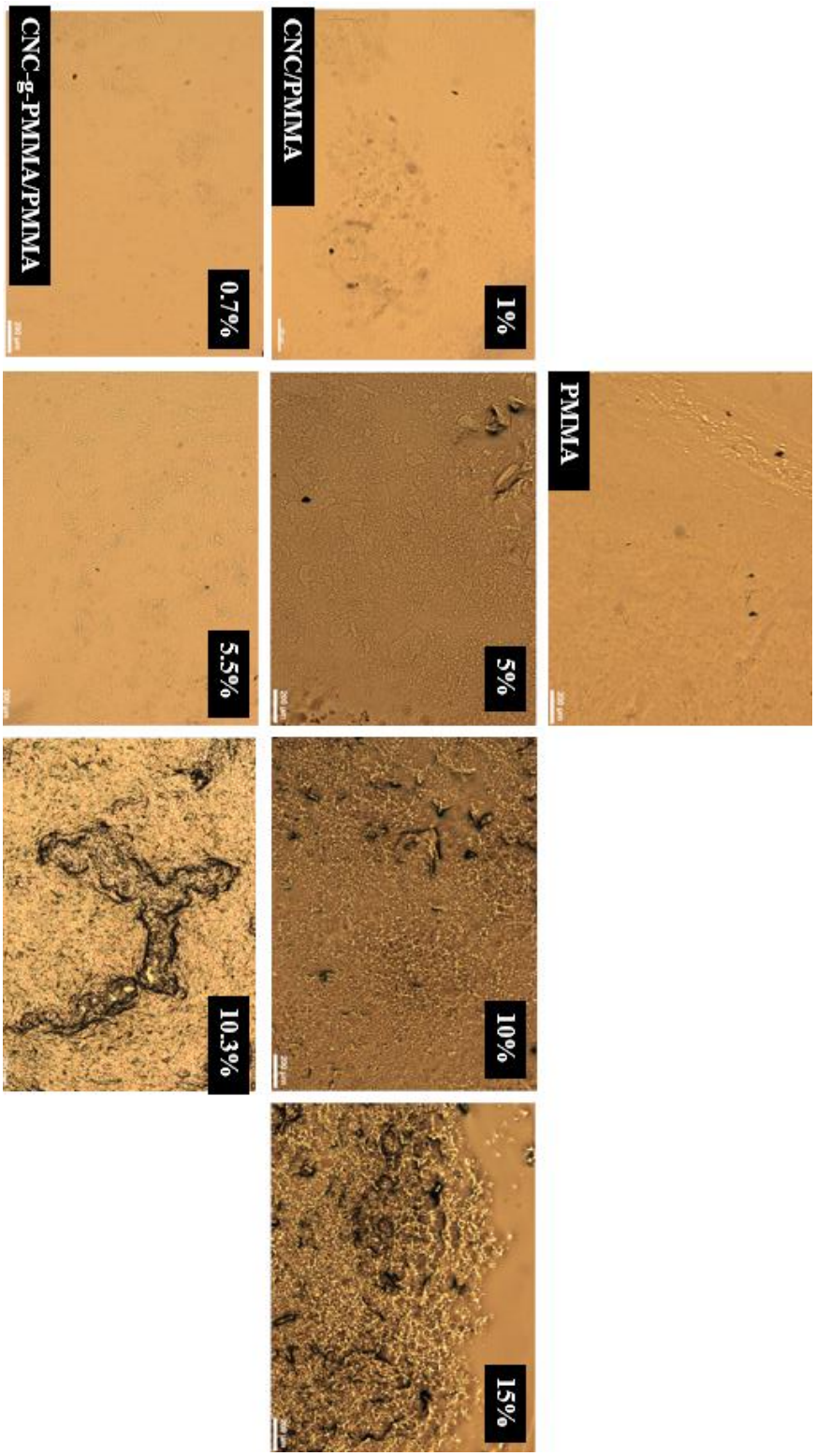

Figure 28. Optical microscope images of PMMA, CNC/PMMA and CNC-g-PMMA/PMMA composites

4.3.2 Mechanical properties of CNC/PMMA and CNC-g-PMMA/PMMA composites

CNC/PMMA and CNC-g-PMMA/PMMA composites were cut into dog bone samples to measure the effect of CNC and CNC-g-PMMA fillers on the stiffness of the material [Figure 29]. If the CNC-g-PMMA had an improved interface with the PMMA matrix, it would be expected that CNC-g-PMMA/PMMA composites would have greater Young's moduli.

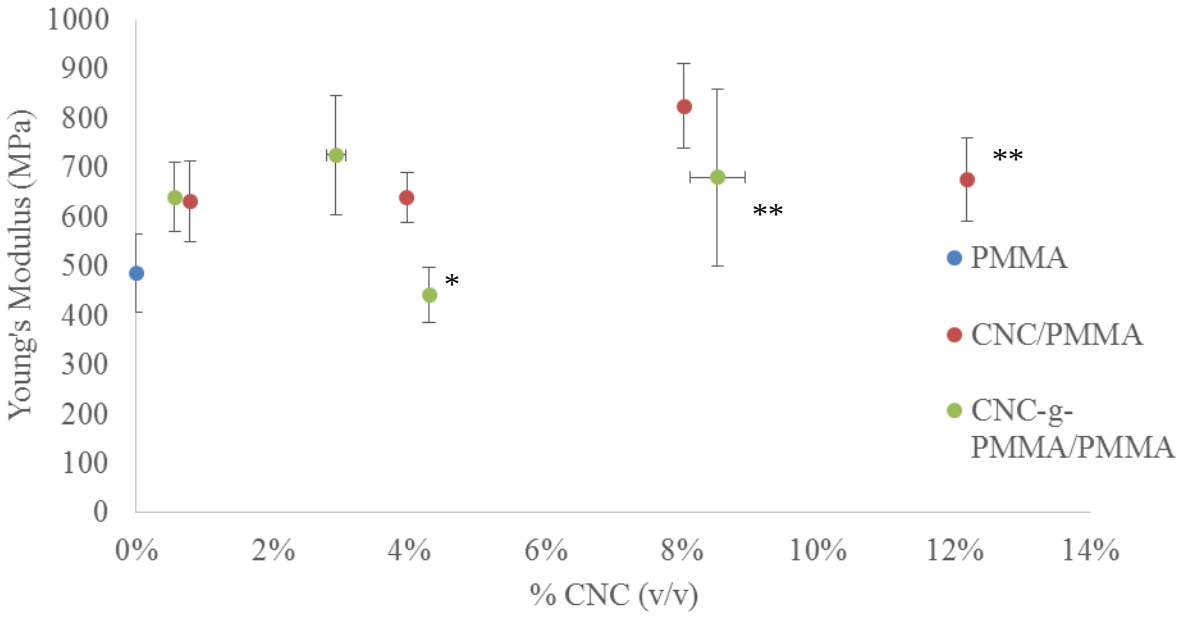

Figure 29. Young's Moduli of PMMA, CNC/PMMA and CNC-g-PMMA/PMMA composites

The Young's moduli of the CNC-g-PMMA/PMMA composites were greater than those of CNC/PMMA at lower volume fractions of CNC, however for higher reinforcement loaded composites, the moduli decreased. All of the composites, with the exception of the 4.3% v/v CNC-g-PMMA/PMMA composite, exhibited higher Young's moduli than the neat PMMA. The 4.3% v/v CNC-g-PMMA/PMMA sample indicated with (*) shows deteriorated mechanical properties because the film was contaminated with dust during the heated press step during the making of the

film. The low modulus of this film should not be attributed to the effect of the modified reinforcement phase. The Young's modulus of the neat PMMA was considerably lower than reported literature values, which suggests that the preparation method of the films could be the cause of the low modulus values [13]. The properties of either the CNC phase or the PMMA matrix could have been compromised by the elevated temperature of the heated press.

The samples indicated with (**) were composites with high percentages of CNC reinforcement. Nanocomposites will usually reach a maximum concentration of reinforcement phase at which they exhibit deteriorated properties compared to lower volume factions because the nanoparticles begin to agglomerate. This seems to happen with the samples of 8% v/v and greater for both CNC-g-PMMA and s.CNC composites. The superior stiffness of the grafted filler to the s.CNC fillers can be best seen between 0.57% and 4% v/v of CNC-g-PMMA and s.CNCs. Since it is difficult to draw a conclusion from only two composite plot points for each filler, more composites with similar concentrations of CNCs variations should be investigated to confirm this trend.

An additional factor to consider when comparing the CNC and CNC-g-PMMA composites is that the grafted polymer on the CNC-g-PMMA is of unknown molecular weight. The CNC-g-PMMA nanocrystals can be between as high as 65% w/w PMMA with a molecular weight that is most likely lower than the PMMA of the matrix. This would most likely have a smaller impact on composites with lower fractions of added CNC-g-PMMA, however it could have a significant influence on composites with higher concentrations of CNC-g-PMMA. For example, a 15% w/w CNC/PMMA composite would be 85% w/w 75000 g/mol PMMA, while a 15% CNC-g-PMMA/PMMA composite (with 65% w/w grafted PMMA) would only have 66% 75000 g/mol

PMMA and 19% w/w PMMA of an lower, unknown molecular weight. In order to better understand the mechanical data, more must be understood about the properties of the grafted polymer.

The change of the interface between the s.CNC and CNC-g-PMMA reinforcements and the PMMA matrix was investigated by fitting the mechanical data with the Shear-Lag Capped (SLC) model [Figure 30] [62].

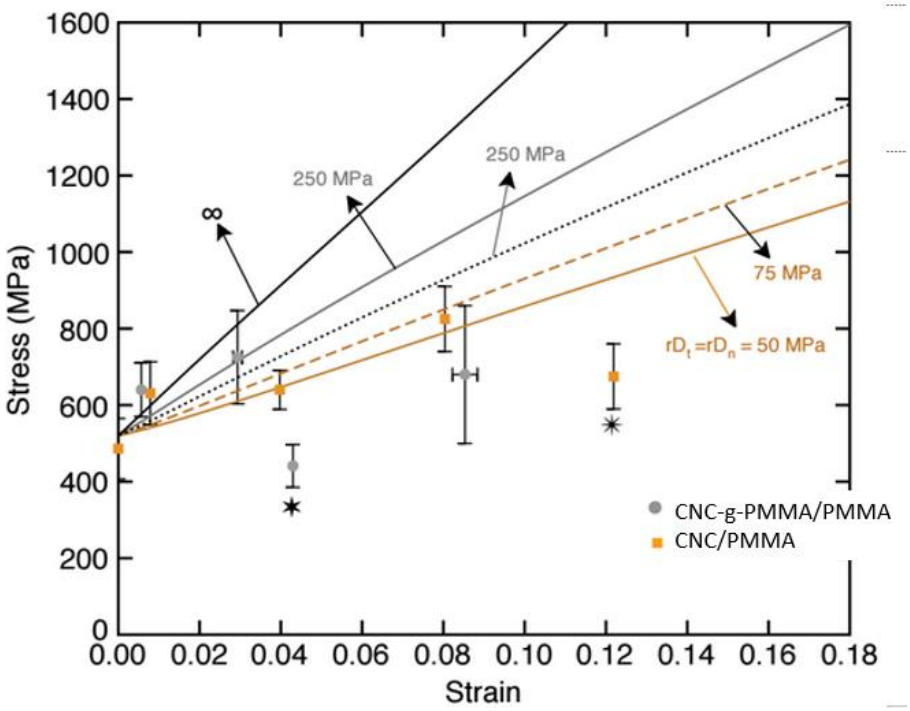

Figure 30. Composite data fitted with SLC model to measure change in reinforcement-matrix interface. Plot made with the help of M. Shir Mohammadi.

The solid line indicates what the properties would be given a perfect interface and steeper slopes indicate a higher interface value and improved compatibility between phases. For the CNC-g-PMMA/PMMA, the interface value seems to be close to 250 MPa for the lower concentrations of nanofillers. The composites with s.CNC had a lower interface value, between 50 MPa and 75 MPa. This model suggests that the grafting of CNCs with PMMA improved the interface of the reinforcement phase and the PMMA matrix.

Overall, the mechanical data collected with these composites cannot be used to measure the interface between the composite phases for either the modified or unmodified reinforcement phases. This is because the results are dominated by the effects of the solvent casting and heated pressing methods. The calculations done with the SLC model show what could be done with the mechanical data of the modified and unmodified CNC composites, however the interface cannot be measured until better prepared samples are made and tested. More samples should also be prepared to allow for statistical analysis to be done on the results.

CHAPTER 5: CONCLUSION

5.1 Modification of CNCs

It was demonstrated through FTIR and elemental analysis that cellulose nanocrystals were successfully modified with an immobilized EDB-inspired photoinitiator. Elemental analysis also showed that the concentration of the initiator could be controlled fairly well using the duration of the reaction. These modified nanocrystals then participated in a photoinitiated polymerization with MMA to make CNC-g-PMMA, which was confirmed with FTIR and elemental analysis. Because the PMMA graft was covalently bonded to the CNCs, CNC-g-PMMA exhibited physical properties in DSC and TGA that were a hybrid of s.CNCs and PMMA. Elemental analysis indicated that the CNC-g-PMMA can be between 40% and 67% w/w grafted PMMA. The amount of attached initiator did not seem to impact the amount of PMMA grafted to the CNC surface, suggesting a more complicated radical reaction than the initiator being the sole site of polymerization. TEM images suggested that the modifications of the CNCs did not significantly

change the sizes or dispersion of the crystals. The grafted PMMA could be detached using cellulase, however these chains were not successfully characterized using JOEL mass spectroscopy. It was determined that this was not the correct method to be used to find molecular weight of the polymer chains.

5.2 PMMA Composites of CNC and CNC-g-PMMA

It was expected that with the addition of polymer chains to the surface of the CNCs would improve the interface between the nanoparticles and the hydrophobic PMMA matrix. An improved interface should lead to better reinforcement dispersion, greater optical clarity and improved mechanical properties, such as stiffness. PMMA composites made with s.CNCs and CNC-g-PMMA were observed under an optical microscope for evidence of agglomeration and lack of clarity. Composites of both types of reinforcements around 1% w/w had appearances very similar to that of neat PMMA. However, at higher amounts of reinforcement the composites appeared cloudy and roughly textured. This could be from increased agglomeration at high filler concentrations. It could also be from air bubbles that are introduced during the acetone solvent casting method. This method could be improved by casting the films in a vacuum to keep the bubbles small.

Composites of s.CNC/PMMA and CNC-g-PMMA/PMMA were tested with a variety amounts of CNCs added to find their Young's moduli and compare the stiffness of these composites to neat PMMA. The nanocomposites all showed increased stiffness compared to neat PMMA, with the exception of one CNC-g-PMMA/PMMA composite that had been compromised with contaminants during the film making process. At lower concentrations of CNCs, the CNC-g-

PMMA/PMMA composites had greater stiffness that the s.CNC/PMMA composites. At higher concentrations of CNCs above 8% w/w , both types of composites had diminished moduli. This occurs with nanocomposites as the concentration of particles becomes too high to maintain proper dispersion and agglomeration occurs. The mechanical data was fit to the SLC model to compare the interface value for the two types of CNCs. With lower amounts of CNCs, the CNC-g-PMMA/PMMA composites had a higher approximated interface value, 250 MPa, than the s.CNC/PMMA composite, between 50 MPa and 75 MPa. This suggests that the interface between the composite phases could have been improved with the polymer graft.

5.3 Future Work

The scope of this project achieved the immobilization and characterization of a photoinitiator onto CNCs, the graft of PMMA onto the nanocrystals and the initial investigation into the mechanical, optical and interface properties of composites made with CNC-g-PMMA. The next steps to continue the work of this project will be to (i) “scale-up” the production of CNC-g-PMMA using process intensification techniques such as the spinning disk reactor, (ii) improve the film making procedure for mechanical and optical testing, (iii) increase the number of samples and the variety of added CNC concentrations in composites for testing and (iv) characterize the grafted polymer in CNC-g-PMMA.

Using a reaction instrument such as the spinning disk reactor would benefit this project because it would allow for larger batches of CNC-g-PMMA to be made, making it possible to formulate more samples to test. The scintillation vial polymerization set-up was extremely

restrictive in the batch sizes that could be performed, resulting in only thin, small composites to be tested. In addition to larger batches, a spinning disk reactor would allow for a great deal more control over light exposure, mixing rate and reaction temperature. These variables were not easily controlled with the scintillation vial set up and could have caused a considerable variation on the grafted product.

With the increase in CNC-g-PMMA batch sizes, more composites could be made and tested to explore the effect of grafting CNCs with PMMA on the composite interface. The initial mechanical data suggest that the most improvement of properties between CNC-g-PMMA and s.CNCs was seen between 0.6% and 4% v/v. More composites should be made within these regions of concentrations to explore how much the grafting effects the interface and mechanical data. More numerous samples prepared with an improved method should be tested to give results that can be modeled with the SCL model to provide information about the difference in modified and unmodified CNCs interface with PMMA.

An improved method of making films would also help isolate the variables of concentration and type of filler. With the current method, there are numerous opportunities to introduce defects such as bubbles and dirt, which will affect the mechanical data particularly in thin films. Casting the films in a vacuum oven could be an improved method because it would shrink bubbles and potentially remove the need to press and melt the samples repeatedly. Making thicker samples would also make the imperfections less influential in the mechanical testing.

Finally, the grafted PMMA must be characterized. During the project, the PMMA was successfully removed from the CNCs through cellulase digestion. The only available instrumentation at the time was JOEL FAB+ Mass Spectroscopy, which was not ideal for the

measurement of PMMA molecular weight. Some techniques that would be more useful could be solid-state NMR end group analysis, MALDI or size-exclusion chromatography. Once the grafted PMMA is characterized, grafts of average molecular weights could be studied and optimized in different composites. It is important to know the size and frequency of the bonded polymers to understand how the modification will change the surface chemistry of the cellulose.

Overall, this project developed a method for photopolymerizing PMMA onto the surface of CNCs, which seems to have improved the interface between the CNCs and PMMA matrix. With further development, this method could be "scaled-up" with process intensification, utilized with a wider range of polymer matrices and grafts and utilized in fields such as automotive, packaging and construction. CNCs are renewable, lightweight, affordable and biodegradable nanoparticles that have a great deal of potential for countless applications. By improving CNCs interface with hydrophobic matrices, the possibilities only grow wider.

Bibliography

[1] H. Charreau, M. L Foresti, and A. Vázquez, “Nanocellulose patents trends: a comprehensive review on patents on cellulose nanocrystals, microfibrillated and bacterial cellulose,” *Recent Pat. Nanotechnol.*, vol. 7, no. 1, pp. 56–80, 2013.
[2] V. Charlot, A. Ibrahim, X. Allonas, C. Croutxe-Barghorn, and C. Delaite, “Photopolymerization of methyl methacrylate: effects of photochemical and photonic parameters on the chain length,” *Polym. Chem.*, vol. 5, no. 21, pp. 6236–6243, 2014.
[3] R. J. Moon, A. Martini, J. Nairn, J. Simonsen, and J. Youngblood, “Cellulose nanomaterials review: structure, properties and nanocomposites,” *Chem. Soc. Rev.*, vol. 40, no. 7, pp. 3941–3994, 2011.
[4] D. N.-S. Hon, “Cellulose: a random walk along its historical path,” *Cellulose*, vol. 1, no. 1, pp. 1–25, 1994.
[5] Y. Habibi, L. A. Lucia, and O. J. Rojas, “Cellulose nanocrystals: chemistry, self-assembly, and applications,” *Chem. Rev.*, vol. 110, no. 6, pp. 3479–3500, 2010.
[6] A. Dufresne, “Polysaccharide nano crystal reinforced nanocomposites,” *Can. J. Chem.*, vol. 86, no. 6, pp. 484–494, 2008.
[7] R. P. Feynman, “There’s plenty of room at the bottom,” *Eng. Sci.*, vol. 23, no. 5, pp. 22–36, 1960.
[8] M. Scheu, V. Veefkind, Y. Verbandt, E. M. Galan, R. Absalom, and W. Förster, “Mapping nanotechnology patents: The EPO approach,” *World Pat. Inf.*, vol. 28, no. 3, pp. 204–211, 2006.
[9] R. F. Nickerson and J. A. Habrle, “Cellulose intercrystalline structure,” *Ind. Eng. Chem.*, vol. 39, no. 11, pp. 1507–1512, 1947.
[10] S. Beck-Candanedo, M. Roman, and D. G. Gray, “Effect of reaction conditions on the properties and behavior of wood cellulose nanocrystal suspensions,” *Biomacromolecules*, vol. 6, no. 2, pp. 1048–1054, 2005.
[11] M. A. Hubbe, O. J. Rojas, L. A. Lucia, and M. Sain, “Cellulosic nanocomposites: a review,” *BioResources*, vol. 3, no. 3, pp. 929–980, 2008.
[12] H. Althues, J. Henle, and S. Kaskel, “Functional inorganic nanofillers for transparent polymers,” *Chem. Soc. Rev.*, vol. 36, no. 9, pp. 1454–1465, 2007.
[13] U. Ali, K. J. B. A. Karim, and N. A. Buang, “A Review of the Properties and Applications of Poly (Methyl Methacrylate)(PMMA),” *Polym. Rev.*, vol. 55, no. 4, pp. 678–705, 2015.
[14] R. Otto and T. Ernst, “Process for the polymerization of methyl methacrylate,” Sep-1939.
[15] Z. J. A. Amer, J. K. Ahmed, and S. F. Abbas, “Chitosan/PMMA bioblend for drug release applications,” *Int. J. Eng. Technol.*, vol. 4, no. 5, 2014.
[16] P. M. Stevens, *Polymer chemistry: an introduction*. New York: Oxford University Press, New York, 1999.
[17] C. Decker, “Kinetic study and new applications of UV radiation curing,” *Macromol. Rapid Commun.*, vol. 23, no. 18, pp. 1067–1093, 2002.
[18] M. G. Neumann, C. C. Schmitt, and M. A. Horn, “The effect of the mixtures of photoinitiators in polymerization efficiencies,” *J. Appl. Polym. Sci.*, vol. 112, no. 1, pp. 129–134, 2009.

[19] D. Hull and T. W. Clyne, *An introduction to composite materials*. Cambridge university press, 1996.
[20] J.-K. Kim and Y.-W. Mai, *Engineered interfaces in fiber reinforced composites*. Elsevier, 1998.
[21] Gordon Armstrong, "An introduction to polymer nanocomposites," *Eur. Jouranl Phys.*, vol. 36, p. 34, 2015.
[22] S. D. Pask, O. Nuyken, and Z. Cai, "The spinning disk reactor: an example of a process intensification technology for polymers and particles," *Polym. Chem.*, vol. 3, no. 10, pp. 2698–2707, 2012.
[23] K. V. Boodhoo and S. R. Al-Hengari, "Micromixing Characteristics in a Small-Scale Spinning Disk Reactor," *Chem. Eng. Technol.*, vol. 35, no. 7, pp. 1229–1237, 2012.
[24] K. V. K. Boodhoo and R. J. Jachuck, "Process intensification: spinning disk reactor for styrene polymerisation," *Appl. Therm. Eng.*, vol. 20, no. 12, pp. 1127–1146, 2000.
[25] K.-Y. Lee, Y. Aitomäki, L. A. Berglund, K. Oksman, and A. Bismarck, "On the use of nanocellulose as reinforcement in polymer matrix composites," *Compos. Sci. Technol.*, vol. 105, pp. 15–27, 2014.
[26] A. Khan, T. Huq, R. A. Khan, B. Riedl, and M. Lacroix, "Nanocellulose-based composites and bioactive agents for food packaging," *Crit. Rev. Food Sci. Nutr.*, vol. 54, no. 2, pp. 163–174, 2014.
[27] N. Lin and A. Dufresne, "Nanocellulose in biomedicine: current status and future prospect," *Eur. Polym. J.*, vol. 59, pp. 302–325, 2014.
[28] V. Favier, G. R. Canova, J. Y. Cavaillé, H. Chanzy, A. Dufresne, and C. Gauthier, "Nanocomposite materials from latex and cellulose whiskers," *Polym. Adv. Technol.*, vol. 6, no. 5, pp. 351–355, 1995.
[29] Y. Li, Q. Fu, S. Yu, M. Yan, and L. Berglund, "Optically Transparent Wood from a Nanoporous Cellulosic Template: Combining Functional and Structural Performance," *Biomacromolecules*, 2016.
[30] H. Dong, K. E. Strawhecker, J. F. Snyder, J. A. Orlicki, R. S. Reiner, and A. W. Rudie, "Cellulose nanocrystals as a reinforcing material for electrospun poly (methyl methacrylate) fibers: Formation, properties and nanomechanical characterization," *Carbohydr. Polym.*, vol. 87, no. 4, pp. 2488–2495, 2012.
[31] E. E. Kiziltas, A. Kiziltas, S. C. Bollin, and D. J. Gardner, "Preparation and characterization of transparent PMMA–cellulose-based nanocomposites," *Carbohydr. Polym.*, vol. 127, pp. 381–389, 2015.
[32] Istvan Siro and David Plackett, "Microfibrillated cellulose and new nanocomposite materials: a review," *Cellulose*, vol. 17, no. 3, pp. 459–494, 2010.
[33] D. Roy, M. Semsarilar, J. T. Guthrie, and S. Perrier, "Cellulose modification by polymer grafting: a review," *Chem. Soc. Rev.*, vol. 38, no. 7, pp. 2046–2064, 2009.
[34] E. Larsson, S. A. Pendergraph, T. Kaldéus, E. Malmström, and A. Carlmark, "Cellulose grafting by photoinduced controlled radical polymerisation," *Polym. Chem.*, vol. 6, no. 10, pp. 1865–1874, 2015.
[35] S. Hansson, P. Antoni, H. Bergenudd, and E. Malmström, "Selective cleavage of polymer grafts from solid surfaces: assessment of initiator content and polymer characteristics," *Polym. Chem.*, vol. 2, no. 3, pp. 556–558, 2011.

[36] J. Zhuo and G. Sun, "Light-induced surface graft polymerizations initiated by an anthraquinone dye on cotton fibers," *Carbohydr. Polym.*, vol. 112, pp. 158–164, 2014.
[37] A. Carlmark and E. Malmström, "Atom transfer radical polymerization from cellulose fibers at ambient temperature," *J. Am. Chem. Soc.*, vol. 124, no. 6, pp. 900–901, 2002.
[38] K. H. Hong, N. Liu, and G. Sun, "UV-induced graft polymerization of acrylamide on cellulose by using immobilized benzophenone as a photo-initiator," *Eur. Polym. J.*, vol. 45, no. 8, pp. 2443–2449, 2009.
[39] Y. Zhang, X. Li, H. Li, M. E. Gibril, K. Han, and M. Yu, "Thermal and rheological properties of cellulose-graft-polyacrylamide synthesized by in situ graft copolymerization," *RSC Adv.*, vol. 3, no. 29, pp. 11732–11737, 2013.
[40] C. R. Routray, B. Tosh, N. Nayak, and others, "Grafting of polymethyl methacrylate onto cellulose acetate in homogeneous medium using ceric (IV) ion as initiator," *Indian J. Chem. Technol.*, vol. 20, no. 3, pp. 202–209, 2013.
[41] M. Coskun and M. M. Temüz, "Grafting studies onto cellulose by atom-transfer radical polymerization," *Polym. Int.*, vol. 54, no. 2, pp. 342–347, Feb. 2005.
[42] K. Littunen, U. Hippi, L.-S. Johansson, M. Österberg, T. Tammelin, J. Laine, and J. Seppälä, "Free radical graft copolymerization of nanofibrillated cellulose with acrylic monomers," *Carbohydr. Polym.*, vol. 84, no. 3, pp. 1039–1047, 2011.
[43] E. Lam, K. B. Male, J. H. Chong, A. C. Leung, and J. H. Luong, "Applications of functionalized and nanoparticle-modified nanocrystalline cellulose," *Trends Biotechnol.*, vol. 30, no. 5, pp. 283–290, 2012.
[44] A. Carlmark, E. Larsson, and E. Malmström, "Grafting of cellulose by ring-opening polymerisation–A review," *Eur. Polym. J.*, vol. 48, no. 10, pp. 1646–1659, 2012.
[45] M. V. Biyani, M. Jorfi, C. Weder, and E. J. Foster, "Light-stimulated mechanically switchable, photopatternable cellulose nanocomposites," *Polym. Chem.*, vol. 5, no. 19, pp. 5716–5724, 2014.
[46] Y. Zheng, J. Song, B. Cheng, X. Fang, and Y. Yuan, "Preparation and flame retardancy of 3-(hydroxyphenylphosphinyl)-propanoic acid esters of cellulose and their fibers," *Cellulose*, vol. 22, no. 1, pp. 229–244, 2015.
[47] H. Kang, R. Liu, and Y. Huang, "Graft modification of cellulose: Methods, properties and applications," *Polymer*, 2015.
[48] Z. Zhang, Q. Wu, K. Song, S. Ren, T. Lei, and Q. Zhang, "Using cellulose nanocrystals as a sustainable additive to enhance hydrophilicity, mechanical and thermal properties of poly (vinylidene fluoride)/poly (methyl methacrylate) blend," *ACS Sustain. Chem. Eng.*, vol. 3, no. 4, pp. 574–582, 2015.
[49] P. Poomalai, T. O. Varghese, and others, "Thermomechanical Behaviour of Poly (methyl methacrylate)/Copoly (ether-ester) Blends," *ISRN Mater. Sci.*, vol. 2011, 2011.
[50] P. Rani, S. Mishra, and G. Sen, "Microwave based synthesis of polymethyl methacrylate grafted sodium alginate: its application as flocculant," *Carbohydr. Polym.*, vol. 91, no. 2, pp. 686–692, 2013.
[51] K. H. Prashanth, K. Lakshman, T. R. Shamala, and R. N. Tharanathan, "Biodegradation of chitosan-graft-polymethylmethacrylate films," *Int. Biodeterior. Biodegrad.*, vol. 56, no. 2, pp. 115–120, 2005.

[52] G. Prasad, K. Prasad, R. Meena, and A. K. Siddhanta, “Facile preparation of Chaetomorpha antennina based porous polysaccharide–PMMA hybrid material by radical polymerization under microwave irradiation,” *J. Mater. Sci.*, vol. 44, no. 15, pp. 4062–4068, 2009.
[53] L. Xue, U. S. Agarwal, and P. J. Lemstra, “High molecular weight PMMA by ATRP,” *Macromolecules*, vol. 35, no. 22, pp. 8650–8652, 2002.
[54] T. Grimaud and K. Matyjaszewski, “Controlled/‘living’ radical polymerization of methyl methacrylate by atom transfer radical polymerization,” *Macromolecules*, vol. 30, no. 7, pp. 2216–2218, 1997.
[55] Z. Guan and B. Smart, “A remarkable visible light effect on atom-transfer radical polymerization,” *Macromolecules*, vol. 33, no. 18, pp. 6904–6906, 2000.
[56] F. Joubert, O. M. Musa, D. R. Hodgson, and N. R. Cameron, “The preparation of graft copolymers of cellulose and cellulose derivatives using ATRP under homogeneous reaction conditions,” *Chem. Soc. Rev.*, vol. 43, no. 20, pp. 7217–7235, 2014.
[57] R. S. Reiner and A. W. Rudie, “.1 Process Scale-Up of Cellulose Nanocrystal Production to 25 kg per Batch at the Forest Products Laboratory,” 2013.
[58] T. K. Ghose, “Measurement of cellulase activities,” *Pure Appl. Chem.*, vol. 59, no. 2, pp. 257–268, 1987.
[59] Y.-T. Hong, A. Barchuk, and M. J. Krische, “Branch-Selective Intermolecular Hydroacylation: Hydrogen-Mediated Coupling of Anhydrides to Styrenes and Activated Olefins,” *Angew. Chem.*, vol. 118, no. 41, pp. 7039–7042, 2006.
[60] B. C. Smith, *Infrared spectral interpretation: a systematic approach*. Boca Raton: CRC press, 1998.
[61] A. Akelah and D. C. Sherrington, “Synthesis of some vinyl derivatives of cellulose and their grafting copolymerization with styrene,” *J. Appl. Polym. Sci.*, vol. 26, no. 10, pp. 3377–3384, 1981.
[62] M. S. Mohammadi, C. Hammerquist, J. Simonsen, and J. A. Nairn, “The fracture toughness of polymer cellulose nanocomposites using the essential work of fracture method,” *J. Mater. Sci.*, vol. 51, no. 19, pp. 8916–8927, 2016.

CHAPTER 6: APPENDICES

Appendix A: Mass Spectroscopy Data for Cellulase Ungrafted PMMA from CNC-g-PMMA

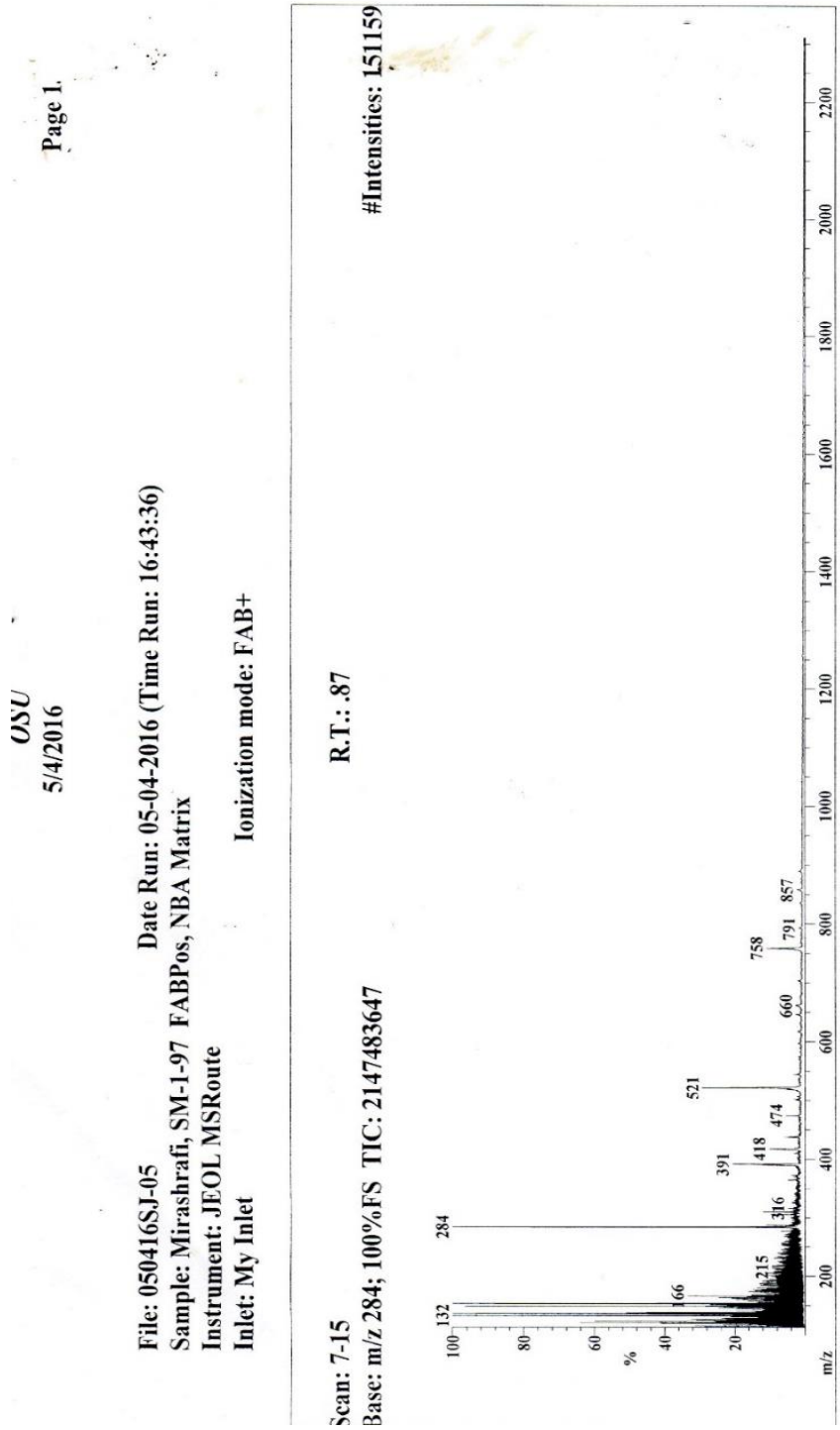

Figure A.1 Mass Spectroscopy of ungrafted PMMA from NBA Matrix

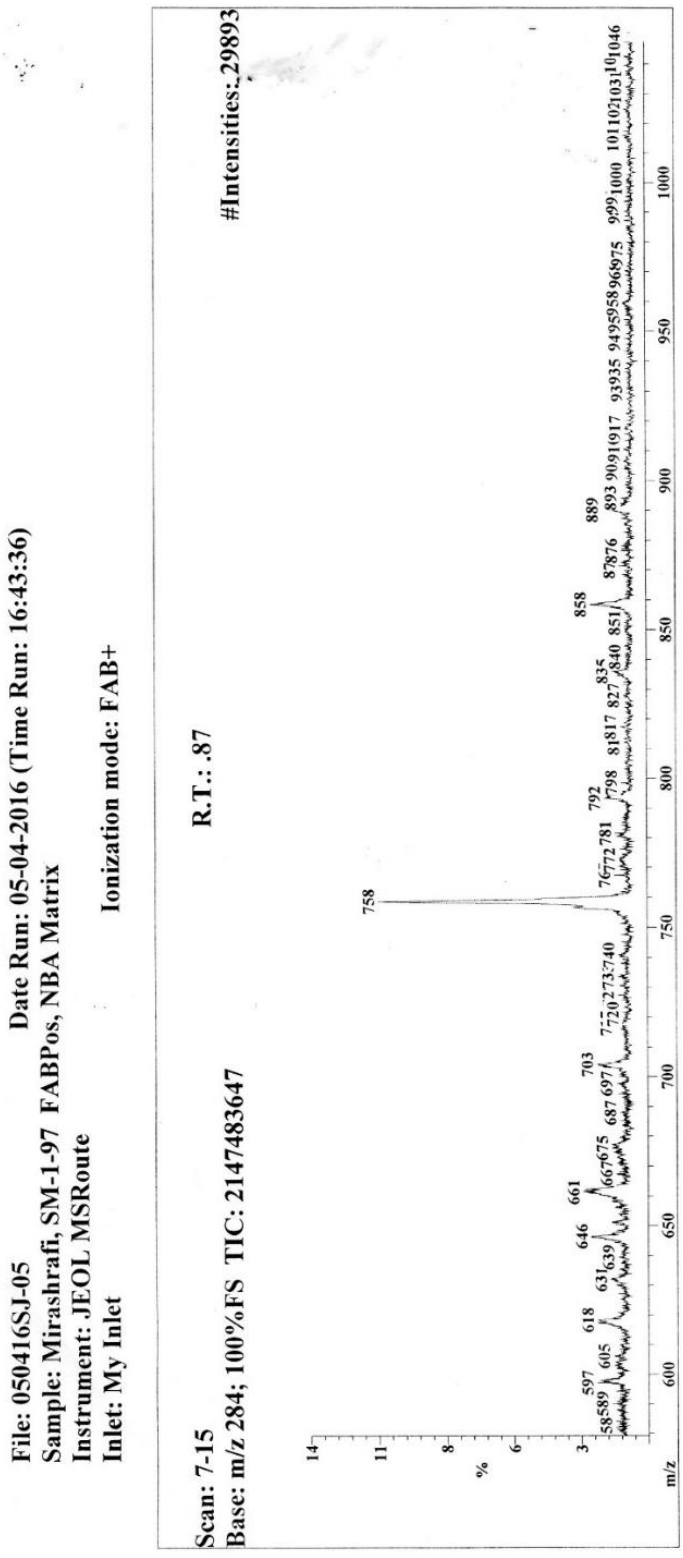

Figure A.2. Mass Spectroscopy of ungrafted PMMA from Glycerol Matrix